



Myc-mediated SDHA acetylation triggers epigenetic regulation of gene expression and tumorigenesis

Shi-Ting Li^{1,8}, De Huang^{1,8}, Shengqi Shen¹, Yongping Cai², Songge Xing¹, Gongwei Wu¹, Zetan Jiang¹, Yijie Hao¹, Mengqiu Yuan^{1,3,4}, Nana Wang², Lianbang Zhu¹, Ronghui Yan¹, Dongdong Yang¹, Lin Wang¹, Zhaoji Liu^{1,3,4}, Xin Hu¹, Rongbin Zhou¹, Kun Qu¹, Ailing Li⁵, Xiaotao Duan⁶✉, Huafeng Zhang¹✉ and Ping Gao^{1,3,4,7}✉

The transcriptional role of cMyc (or Myc) in tumorigenesis is well appreciated; however, it remains to be fully established how extensively Myc is involved in the epigenetic regulation of gene expression. Here, we show that by deactivating succinate dehydrogenase complex subunit A (SDHA) via acetylation, Myc triggers a regulatory cascade in cancer cells that leads to H3K4me3 activation and gene expression. We find that Myc facilitates the acetylation-dependent deactivation of SDHA by activating the SKP2-mediated degradation of SIRT3 deacetylase. We further demonstrate that Myc inhibition of SDH-complex activity leads to cellular succinate accumulation, which triggers H3K4me3 activation and tumour-specific gene expression. We demonstrate that acetylated SDHA at Lys 335 contributes to tumour growth in vitro and in vivo, and we confirm increased tumorigenesis in clinical samples. This study illustrates a link between acetylation-dependent SDHA deactivation and Myc-driven epigenetic regulation of gene expression, which is critical for cancer progression.

The oncogenic transcription factor cMyc (or Myc) regulates up to 15% of the human genes involved in the cell cycle and cellular growth, apoptosis, differentiation and metabolism, as well as other key events, under diverse conditions^{1–3}. Given the diverse functions of the genes regulated by Myc, it is not surprising that deregulated expression of Myc contributes to 30–50% of human malignancies^{4,5}. Myc regulates the expression of many genes transcriptionally by directly binding to the E-boxes on their promoter regions^{6,7}. Recent evidence has emerged that reveals the involvement of Myc in the epigenetic regulation of gene expression in human malignancies^{8–10}, but the underlying mechanisms remain to be fully established. For instance, several groups have independently reported that the level of trimethylated histone H3 Lys 4 (H3K4me3), which is often found surrounding the transcriptional start sites of active genes^{11–13}, is enriched within promoter regions of Myc-targeted genes^{8,14}. However, it is still unclear whether Myc itself is actively involved in facilitating H3K4me3 modification and the subsequent epigenetic regulation of gene expression.

Protein acetylation on lysine residues was initially identified as a major post-translational modification of histones. Recent studies have also identified acetylated non-histone proteins and acetylation-modifying enzymes outside the nucleus for potential regulation of a wide range of cellular processes^{15,16}. Moreover, a large number of acetylation-modifying enzymes that catalyse intermediate metabolism have been discovered to directly affect enzyme activity and/

or stability, which is critical for metabolic regulation in response to alterations of extracellular nutrient availability^{17,18}. Notably, increasing evidence has demonstrated that regulation of the reversible acetylation of metabolic enzymes is involved in modulating cancer-cell metabolism, an emerging hallmark of tumorigenesis^{19,20}. However, little is known about the regulatory factor(s) involved in modulating lysine acetylation-mediated metabolic reprogramming and tumour progression.

SDH, as a mitochondrial-inner-membrane-bound enzyme complex, catalyses the oxidation of succinate to fumarate, accompanied by the reduction of ubiquinone to ubiquinol. Germline or somatic mutations of the five genes encoding each subunit of the SDH complex (SDHA, SDHB, SDHC, SDHD and SDHAF2) are frequently found in many human cancers^{21–24}. The SDH mutant predisposes the carrier to renal-cell carcinoma, and a loss of SDH expression is observed in approximately 3% of breast cancers^{25,26}. Dysfunction or mutation of the SDHA, SDHB, SDHC and SDHD or the AF2 subunit results in the accumulation of cellular succinate, which is structurally similar to α -ketoglutarate (α -KG), leading to the inhibition of α -KG-dependent dioxygenase, such as Jumonji-C domain-containing HDMs (JHDMs), and subsequent regulation of gene expression^{27–30}. Although the presence of loss-of-function mutations in the *SDH* gene is a risk factor for malignancy and a poor prognosis, it remains largely unknown whether other means exist to regulate SDH function. For instance, we still do not know whether the loss

¹Division of Molecular Medicine, Hefei National Laboratory for Physical Sciences at Microscale, The CAS Key Laboratory of Innate Immunity and Chronic Disease, School of Life Sciences and Medical Center, University of Science and Technology of China, Hefei, China. ²Department of Pathology, School of Medicine, Anhui Medical University, Hefei, China. ³Guangzhou First People's Hospital, School of Medicine, Institutes for Life Sciences, South China University of Technology, Guangzhou, China. ⁴School of Biomedical Sciences and Engineering, Guangzhou International Campus, South China University of Technology, Guangzhou, China. ⁵Institute of Basic Medical Sciences, National Center of Biomedical Analysis, Beijing, China. ⁶State Key Laboratory of Toxicology and Medical Countermeasures, Beijing Institute of Pharmacology and Toxicology, Beijing, China. ⁷Guangzhou Regenerative Medicine and Health Guangdong Laboratory, Guangzhou, China. ⁸These authors contributed equally: Shi-Ting Li, De Huang. ✉e-mail: xduan@nca.ac.cn; hzhang22@ustc.edu.cn; pgao2@ustc.edu.cn

of function of SDH is facilitated by specific factor(s), rather than SDHA mutations during cancer progression. In this study, we discovered that Myc facilitates the acetylation-dependent deactivation of SDHA by activating SKP2-mediated degradation of SIRT3, which results in accumulation of cellular succinate, facilitating H3K4me3-mediated tumour-specific gene expression. Collectively, our study reveals that acetylation-dependent SDH-complex deactivation is critical for Myc-driven epigenetic regulation of gene expression and tumorigenesis.

Results

Myc inhibits SDH-complex activity and causes cellular succinate accumulation by inducing SDHA acetylation. Several lines of evidence suggest that lysine acetylation plays an important role in the regulation of cancer metabolism and tumorigenesis; however, little is known regarding the regulatory factor(s) involved in this modification. Thus, we set out to determine whether Myc regulates protein lysine acetylation in human cancer cells. We used human B cell line P493 cells carrying a tetracycline-repressible Myc transgene, in which tetracycline treatment results in rapid repression of Myc⁷. A western blot revealed that suppression of Myc by tetracycline treatment marginally affected the global protein acetylation in P493 cells (Fig. 1a). However, using the isolated mitochondrial protein from P493 cells (Extended Data Fig. 1a), we found that the lysine-acetylation modification was significantly decreased by suppression of Myc (Fig. 1a). To identify the protein acetylation regulated by Myc, we analysed mitochondrial acetylated peptides from P493 cells, with or without tetracycline treatment, by nanoscale liquid chromatography separation and high-resolution mass spectrometry analysis (nano LC-MS/MS), respectively (Extended Data Fig. 1b). The nano LC-MS/MS identified 455 lysine-acetylated peptides, which matched 133 distinct proteins with high Myc expression; in contrast, only 173 acetylated peptides matching 72 kinds of mitochondrial proteins in Myc-depleted P493 cells were

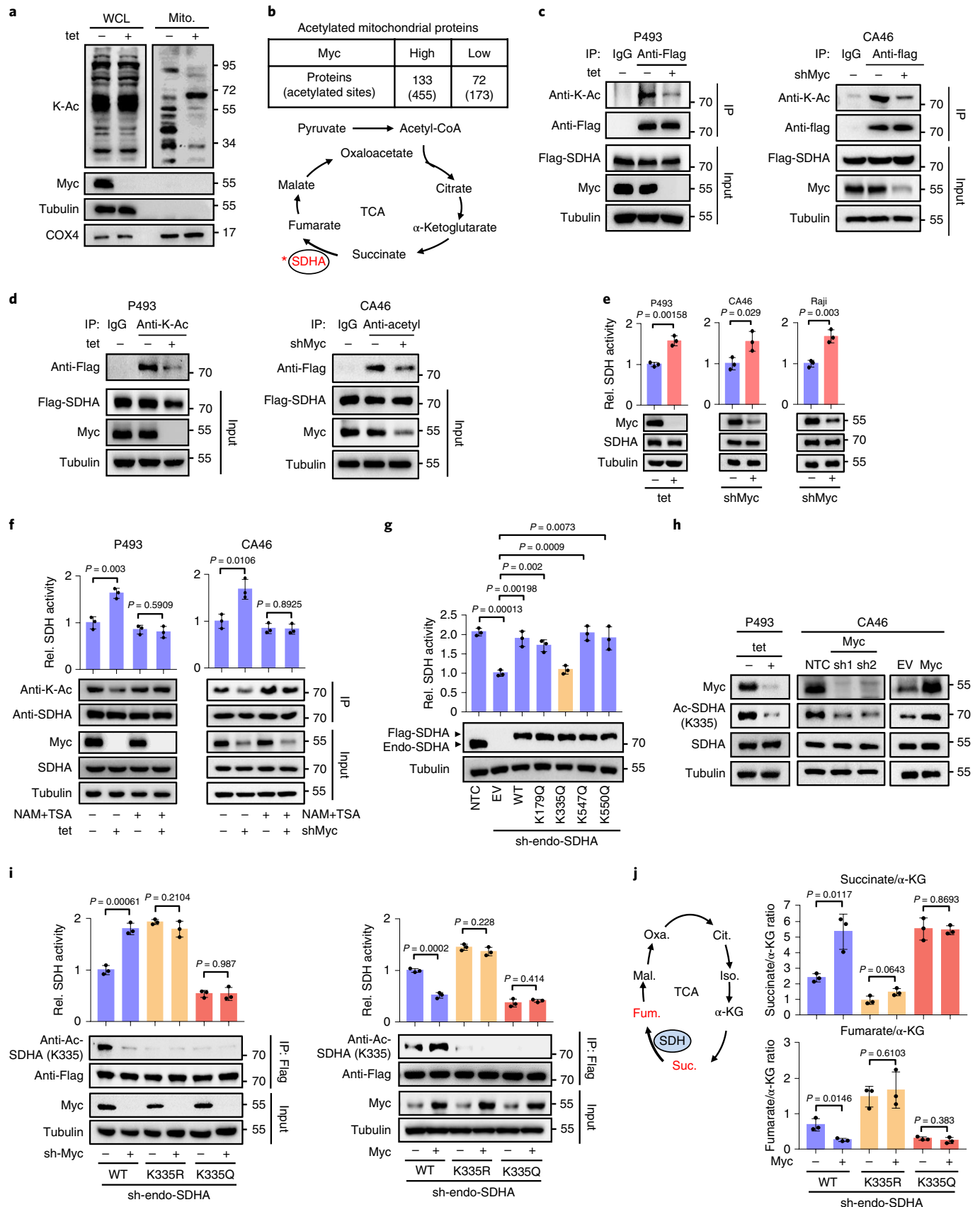
recovered (Fig. 1b and Supplementary Table 1). These nano LC-MS/MS data were consistent with the western blot results showing a broad Myc-induced promotion of the acetylation of mitochondrial proteins (Fig. 1a).

Furthermore, most of the enzymes in the tricarboxylic acid (TCA) cycle exhibited high levels of lysine-acetylation modification (Supplementary Table 2). Among these enzymes, acetylation modification of SDHA was closely correlated with Myc expression in P493 cells (Fig. 1c and Supplementary Table 2). The immunoprecipitation assay showed that lysine-acetylated exogenous [EYKEEEK]₂-14-amino-acid carboxy-terminal extension (Flag)-tagged SDHA was markedly decreased by suppression of Myc with tetracycline in P493 cells or with short hairpin RNAs (shRNAs) in CA46 or HT1080 cells (Fig. 1c and Extended Data Fig. 1c, left). Reverse immunoprecipitation using anti-acetylated-lysine revealed that inhibition of Myc dramatically reduced lysine acetylation of SDHA (Fig. 1d and Extended Data Fig. 1c, right). Lysine-acetylation modification on many enzymes has been reported to affect their enzyme activities^{31–33}. Considering that Myc enhanced acetylation of SDHA, the major component of the succinate dehydrogenase (SDH) complex, we next investigated whether Myc could modulate SDH activity. Interestingly, suppression of Myc significantly enhanced SDH complex activity in different cell lines (Fig. 1e and Extended Data Fig. 1d). In contrast, overexpression of Myc suppressed SDH complex activity in both HT1080 and HeLa cells (Extended Data Fig. 1d), suggesting that Myc negatively regulates SDH complex activity in different types of tumour cells. To examine whether Myc regulates SDH complex activity by modulating lysine acetylation on SDHA, we treated the cells with trichostatin A (TSA), an inhibitor of histone deacetylase, and nicotinamide (NAM), an inhibitor of the SIRT deacetylase family. Treatment with TSA and NAM completely blocked the inhibitory effect of tetracycline or shMyc on SDHA acetylation in P493, CA46 and HT1080 cells (Fig. 1f, bottom,

Fig. 1 | Myc inhibits SDH-complex activity and causes cellular succinate accumulation by inducing SDHA acetylation. **a**, Western blot analysis of lysine-acetylation (K-Ac) of proteins in whole-cell lysates (WCL) or mitochondrial lysates (Mito) in P493 cells treated with or without tetracycline (tet) for 48 h. **b**, Analysis of acetylated mitochondrial proteins and their acetylated sites from nano LC-MS/MS. Lysine acetylation sites in SDHA (marked) were closely correlated with Myc expression in P493 cells. **c**, P493 cells stably expressing Flag-SDHA were further treated with or without tetracycline for 48 h (left), or CA46 cells stably expressing Flag-SDHA were further infected with viruses for expression of non-targeting control (NTC) or Myc shRNA (right), followed by immunoprecipitation using anti-flag antibody or IgG and western blot analysis of Flag-SDHA and Myc expression. **d**, P493 cells stably expressing Flag-SDHA were treated with or without tetracycline for 48 h (left), or CA46 cells stably expressing Flag-SDHA were infected with viruses for expression of NTC or Myc shRNA (right), followed by immunoprecipitation assay using anti-lysine-acetylation antibody (anti-K-Ac) or IgG. Myc and Flag-SDHA expression were analysed by western blot. **e**, SDH activity was measured in P493 cells treated with or without tetracycline for 48 h or in CA46 or Raji cells infected with viruses for expression of NTC or Myc shRNA for 48 h. Myc and SDHA expression were analysed by western blotting. Data are presented as the mean \pm s.d. of 3 independent experiments ($n=3$). Group differences are analysed by the two-tailed Student's *t* test. $P < 0.05$ compared with the NTC group. **f**, SDH activity was measured in P493 cells treated with or without tetracycline and further exposed to 10 mM nicotinamide (NAM) and 1 μ M trichostatin A (TSA) (left) or in CA46 cells infected with viruses for expression of NTC or Myc shRNA (right) and further exposed to 10 mM NAM and 1 μ M TSA. Immunoprecipitation assay using anti-SDHA antibody was performed using the above conditions. SDH activity was normalized to protein content. Data are presented as the mean \pm s.d. of 3 independent experiments ($n=3$). Group differences are analysed by the two-tailed Student's *t* test. $P < 0.05$ compared with the corresponding control group; n.s., not significant. **g**, HEK293T cells with stable knockdown of endogenous SDHA were further transfected with empty vector (EV) or vectors expressing Flag-wild-type-SDHA (WT), Flag-SDHA-K179Q (K179Q), Flag-SDHA-K335Q (K335Q), Flag-SDHA-K547Q (K547Q) or Flag-SDHA-K550Q (K550Q), followed by western blot and SDH-activity measurements. Data are presented as the mean \pm s.d. of three independent experiments ($n=3$). Group differences are analysed by the two-tailed Student's *t* test. $P < 0.05$ compared with the NTC group; $P < 0.05$ compared with the EV control group. **h**, Western blot analysis of Myc, SDHA Lys 335 acetylation and endogenous SDHA levels in P493 cells treated with or without tetracycline for 48 h or in CA46 cells expressing NTC or Myc shRNAs (sh1 and sh2), or in CA46 cells expressing pMX-GFP empty vector (EV) or pMX-GFP-Myc vector. **i**, HT1080 cells with a stable knockdown of endogenous SDHA were subsequently infected with viruses for expression of Flag-wild-type-SDHA (WT), Flag-SDHA-K335R (K335R) or Flag-SDHA-K335Q (K335Q). The above cells were further infected with viruses for expression of NTC or Myc shRNA (left) or pMX-GFP empty vector (EV) or pMX-GFP-Myc (right), followed by the measurement of SDH enzyme activity and western blot analysis of SDHA Lys 335 acetylation, flag-SDHA and Myc. Data are presented as the mean \pm s.d. of three independent experiments ($n=3$). Group differences are analysed by the two-tailed Student's *t* test. $P < 0.05$ compared with the corresponding control group. **j**, Cellular succinate, fumarate or α -KG levels were determined by LC-MS in the HT1080 cells used in **i** (right), then the succinate/ α -KG ratio or fumarate/ α -KG ratio was calculated. Data are presented as the mean \pm s.d. of 3 independent experiments ($n=3$). Group differences are analysed by the two-tailed Student's *t* test. $P < 0.05$ compared between indicated groups. $n=3$ independent experiments were repeated with similar results (**a**, **c**, **d** and **h**). Tubulin or COX4 served as the loading control. SDH activities or succinate, fumarate and α -KG levels were normalized to cellular protein. See also Extended Data Fig. 1.

and Extended Data Fig. 1e, bottom). Notably, SDH activity analysis demonstrated that the enhanced SDH complex activity by Myc suppression was attenuated by TSA and NAM treatment

(Fig. 1f, top, and Extended Data Fig. 1e, top), indicating that Myc-mediated SDHA acetylation is involved in its suppression of SDH-complex activity.



Mass spectrum analysis revealed that Lys 335, Lys 547 and Lys 550 of SDHA were potential acetylation sites by Myc (Extended Data Fig. 1f). However, the online database at www.phosphosite.org predicted one putative acetylation site (Lys 179) in SDHA. To identify the lysine residue(s) on SDHA that are protein responsible for its acetylation and activity, we mutated the four residues, that is Lys 179, Lys 335, Lys 547 and Lys 550, to acetyl-mimetic glutamine (Q) and examined their enzyme activity. Knockdown of endogenous SDHA, as expected, significantly inhibited SDH-complex activity, which was recovered by overexpression of the shRNA-resistant wild-type SDHA and the K179Q, K547Q and K550Q mutants, but not the K335Q mutant (Fig. 1g), suggesting that Lys 335 is a potential acetylation site on SDHA that is important for SDH complex activity. The acetylated Lys 335 of SDHA was also shown in our LC-MS/MS map (Extended Data Fig. 1g). It should be noted that K335 on SDHA is evolutionarily conserved from *Escherichia coli* to mammals (Extended Data Fig. 1h). Next, we generated an antibody that specifically recognizes Lys 335-acetylated SDHA, and its specificity was verified by dot blot assay (Extended Data Fig. 1i). Western blot analysis using this antibody showed that Lys 335-acetylated endogenous SDHA was attenuated by suppressing Myc, whereas overexpression of Myc enhanced SDHA Lys 335 acetylation in cancer-cell lines (Fig. 1h and Extended Data Fig. 1j), thus confirming that Lys 335 is the acetylated residue on SDHA by Myc. To address whether Myc represses SDH complex activity by modulating Lys 335 acetylation on SDHA, we knocked down endogenous SDHA and restored the expression of wild-type SDHA as well as K335Q (acetyl-mimetic) and K335R (non-acetylatable arginine (R) substitution) mutants in HT1080 cells. Our data revealed that cells expressing the SDHA K335R mutant exhibited high SDH activity, while cells expressing the K335Q mutant possessed low SDH activity (Fig. 1i). In contrast to the inhibitory effect of Myc on WT SDHA-induced SDH-complex activity, neither shMyc nor overexpression of Myc affected SDHA K335R- or K335Q-mediated SDH activity (Fig. 1i). Taken together, these results demonstrate that Myc inhibits SDH-complex activity by acetylating SDHA at the Lys 335 site.

Since SDH activity is important for the conversion of succinate to fumarate in the TCA cycle (Fig. 1j, left), we next studied cellular succinate, fumarate and α -KG. As expected, knockdown of endogenous SDHA led to increased succinate and decreased fumarate levels in HT1080 cells (Extended Data Fig. 1k). Furthermore, the restoration of SDHA WT and K335R-mutant expression, but not that of the K335Q

mutant, significantly decreased cellular succinate while increasing the fumarate level in HT1080 cells expressing shSDHA (Extended Data Fig. 1l). LC-MS/MS revealed that the restoration of SDHA WT and K335R-mutant expression, but not that of the K335Q mutant, led to a decreased cellular succinate/ α -KG ratio and an increased cellular fumarate/ α -KG ratio (Fig. 1j, right), suggesting an enhanced conversion of succinate to fumarate in those cells. Importantly, ectopically expressed Myc suppressed the WT SDHA-mediated succinate catabolism; however, Myc overexpression showed no effect on either cellular succinate/ α -KG ratio or fumarate/ α -KG ratio in K335R- or K335Q-expressing HT1080 cells (Fig. 1j, right), which is consistent with the SDH-complex activity data (Fig. 1i). In addition, the variations of absolute concentration of cellular succinate and fumarate levels were also similar to the succinate/ α -KG ratio and fumarate/ α -KG ratio (Extended Data Fig. 1m). Metabolite measurements with a biochemical kit displayed similar results (Extended Data Fig. 1n,o). Taken together, our data demonstrate that Myc represses SDH-complex activity by facilitating Lys 335 acetylation on SDHA, leading to the accumulation of succinate in cancer cells.

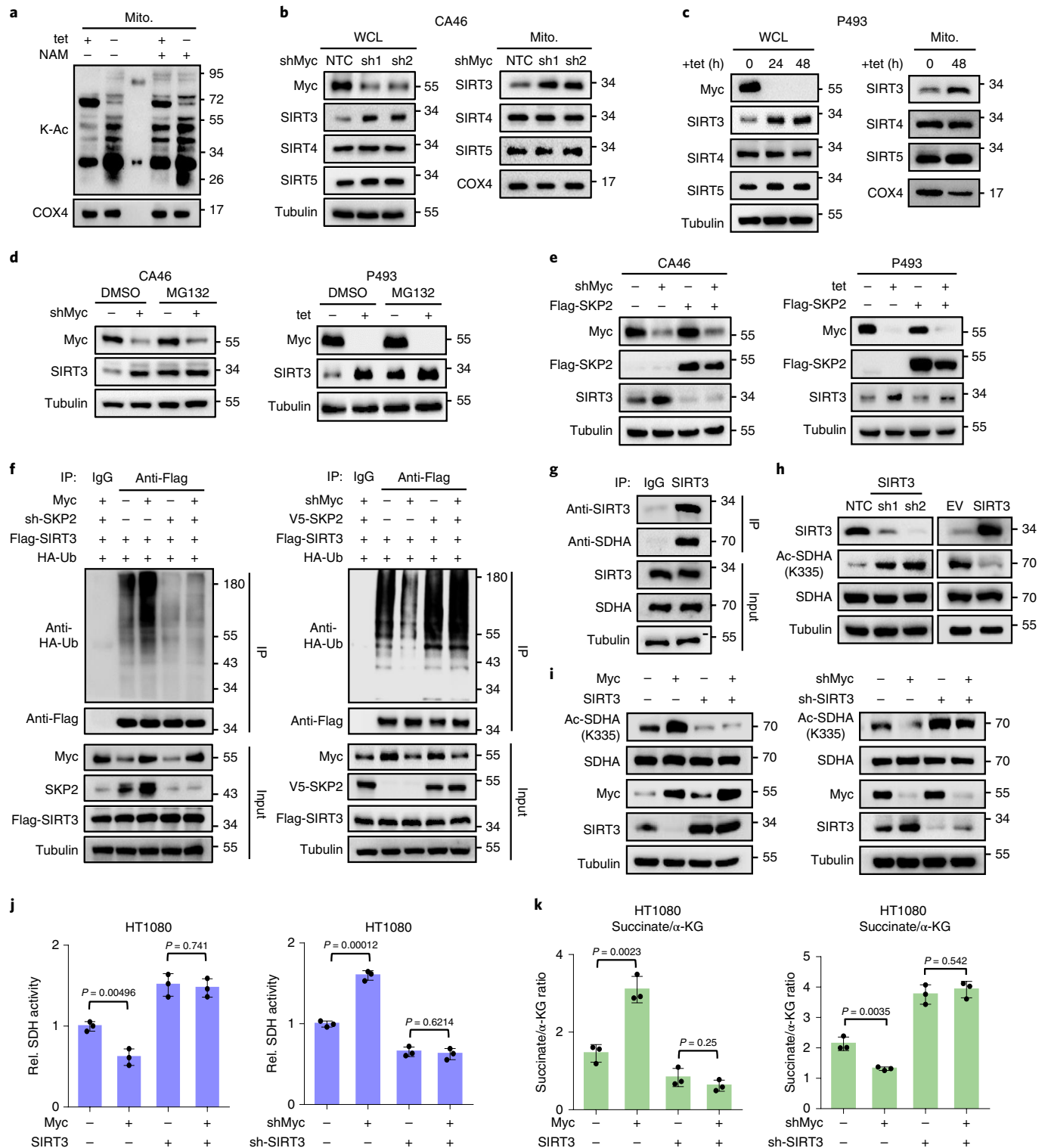
Myc increases SDHA acetylation by accelerating SKP2-mediated proteasomal degradation of SIRT3. To address the mechanisms underlying Myc-induced SDHA lysine-acetylation, we first tested whether Myc regulates deacetylases. Treatment with the SIRT inhibitor NAM, but not with the HDAC inhibitor TSA, significantly increased lysine acetylation of mitochondrial proteins in Myc-depleted P493 cells (Fig. 2a and Extended Data Fig. 2a), indicating that the SIRT family of deacetylases are involved in Myc-regulated lysine acetylation of mitochondrial proteins. Next, we tested all three mitochondrial SIRT deacetylases (SIRT3, SIRT4 and SIRT5) in both CA46 and P493 cells. Western blot analysis of whole-cell lysates and mitochondrial-fraction samples showed that SIRT3 protein was significantly increased by depletion of Myc (Fig. 2b,c). However, SIRT3 messenger RNA levels were not regulated by Myc (Extended Data Fig. 2b). Furthermore, treatment with the proteasome inhibitor MG132 or lactacystin attenuated the suppressive effect of Myc on cells expressing SIRT3 protein (Fig. 2d and Extended Data Fig. 2c), suggesting that Myc stimulates proteasome-dependent SIRT3 degradation. Consistent with previous reports^{34,35}, our data also showed that SIRT3 bound to SKP2, a critical component of the E3 ligase complex (Extended Data Fig. 2d), and that SKP2 is a direct transcriptional target of Myc (Extended Data Fig. 2e,f). Notably, we found

Fig. 2 | Myc increases SDHA acetylation by accelerating SKP2-mediated proteasomal degradation of SIRT3. **a**, Western blot analysis of lysine acetylation in mitochondrial proteins of P493 cells treated with or without tetracycline for 48 h, and further cultured in the presence of vehicle or 10 mM NAM for 6 h. **b**, Western blot analysis of SIRT3, SIRT4 and SIRT5 expression in whole-cell lysates in P493 cells treated with tetracycline for 0, 24 or 48 h (left), or in mitochondrial lysates in P493 cells treated with tetracycline for 0 or 48 h (right). **c**, Western blot analysis of SIRT3, SIRT4 and SIRT5 expression in whole-cell lysates or mitochondrial lysates in CA46 cells infected with viruses for expression of NTC or Myc shRNA for 48 h. **d**, CA46 cells infected with viruses for expression of NTC or Myc shRNA and P493 cells treated with or without tetracycline for 48 h were further cultured in the presence of DMSO or 5 μ M MG132 for 8 h, followed by western blot analysis of Myc and SIRT3 expression. **e**, P493 cells treated with or without tetracycline for 48 h or CA46 cells expressing NTC or Myc shRNA were further infected with EV or pSIN-3xFlag-SKP2 vector, followed by western blot analysis of Myc, Flag-SKP2 and SIRT3 expression. Tubulin served as a loading control. **f**, HEK293T cells expressing Flag-SIRT3 and hemagglutinin-tagged ubiquitin (Ha-Ub) were co-transfected with EV or Myc, and NTC or SKP2 shRNA (left) or co-transfected with NTC or Myc shRNA, and EV or V5-SKP2 (right) for 48 h and treated with 5 μ M MG132 for 8 h before collection. Immunoprecipitation was performed using anti-Flag antibody or IgG using the above cells. Polyubiquitination of Flag-SIRT3 were detected by western blot. **g**, Immunoprecipitation was performed using anti-SIRT3 antibody or IgG in HT1080 cells. SDHA and SIRT3 expression were determined by western blot. **h**, Western blot analysis of SDHA Lys 335 acetylation, SIRT3 and SDHA in HT1080 cells transfected with NTC or SIRT3 shRNAs (sh1 and sh2), or in HT1080 cells transfected with pSIN empty vector or pSIN-SIRT3. **i**, HT1080 cells stably expressing pSIN empty vector or pSIN-SIRT3 were subsequently infected with viruses of pMX-GFP empty vector (EV) or pMX-GFP-Myc (left), or HT1080 cells stably expressing NTC or SIRT3 shRNA were further infected with viruses for expression of NTC or Myc shRNA (right), followed by western blot analysis of Myc, SIRT3, SDHA and SDHA Lys 335 acetylation. **j**, SDH activity was measured using detection kits in the HT1080 cells used in **i**. Relative enzyme activities of triplicate experiments (mean \pm s.d.) are presented ($n=3$). Group differences are analysed by the two-tailed Student's *t* test. $P < 0.05$ compared with the corresponding control group. **k**, Cellular succinate or α -KG levels were determined using LC-MS in HT1080 cells used in **i**, then succinate/ α -KG ratio was calculated. Data are presented as the mean \pm s.d. of 3 independent experiments ($n=3$). Group differences are analysed by the two-tailed Student's *t* test. $P < 0.05$ compared with the corresponding control group. $n=3$ independent experiments were repeated with similar results (**a-i**). Tubulin or COX4 served as the loading control. SDH activities or succinate and α -KG levels were normalized to cellular protein. See also Extended Data Fig. 2.

that knockdown of SKP2 significantly increased SIRT3 expression, whereas overexpression of SKP2 inhibited SIRT3 in different cell lines (Extended Data Fig. 2g), indicating that SKP2 promotes SIRT3 degradation. Moreover, forced expression of SKP2 attenuated the Myc-suppression-induced increase of SIRT3 protein (Fig. 2e and Extended Data Fig. 2h), while knockdown of SKP2 abolished the inhibitory effect of Myc on SIRT3 protein level (Extended Data Fig. 2i) The immunoprecipitation experiment showed that Myc overexpression increased ubiquitination of SIRT3, which was attenuated by knockdown of SKP2 (Fig. 2f, left). In contrast, overexpression of

SKP2 blunted the inhibitory effect of shMyc on SIRT3 ubiquitination (Fig. 2f, right), validating that Myc decreases SIRT3 protein by enhancing its SKP2-mediated proteasome degradation.

Our results further showed that both exogenous and endogenous SDHA interacted with SIRT3 protein (Fig. 2g and Extended Data Fig. 2j). Furthermore, knockdown of SIRT3 markedly increased Lys 335 acetylation on SDHA, while overexpression of SIRT3 reduced Lys 335-acetylated SDHA (Fig. 2h). More importantly, overexpression of SIRT3 abolished Myc-induced SDHA Lys 335 acetylation, while knockdown of SIRT3 attenuated the inhibitory effect of



Myc suppression on Lys 335-acetylated SDHA in HT1080 cells (Fig. 2i). Similar results were also observed in CA46 and P493 cells (Extended Data Fig. 2k,l), demonstrating that SIRT3 is involved in Myc-regulated Lys 335 acetylation on SDHA protein. Finally, we investigated whether SIRT3 participated in Myc-regulated SDH-complex activity to modulate the cellular succinate level and succinate/ α -KG ratio. As shown in Fig. 2j, forced expression of SIRT3 recovered Myc-suppressed SDH-complex activity, whereas knockdown of SIRT3 diminished the promoting effect of Myc depletion on SDH-complex activity in HT1080 cells. Overexpression of SIRT3 relieved Myc-induced cellular succinate accumulation (Extended Data Fig. 2m), and blocked succinate/ α -KG ratio elevation (Fig. 2k, left, and Extended Data Fig. 2n), echoing the enhanced SDH-complex activity in converting succinate to fumarate in cells. In contrast, knockdown of SIRT3 diminished the inhibitory effect of Myc depletion on succinate level (Extended Data Fig. 2o) and promoted elevation of the succinate/ α -KG ratio in HT1080 cells (Fig. 2k, right, and Extended Data Fig. 2p). Similar results were also observed in CA46 and P493 cells (Extended Data Fig. 2q–x). Taken together, these data demonstrate that Myc enhances SDHA Lys 335 acetylation by promoting SKP2-mediated SIRT3 degradation, which consequently suppresses SDH-complex activity and leads to cellular succinate accumulation.

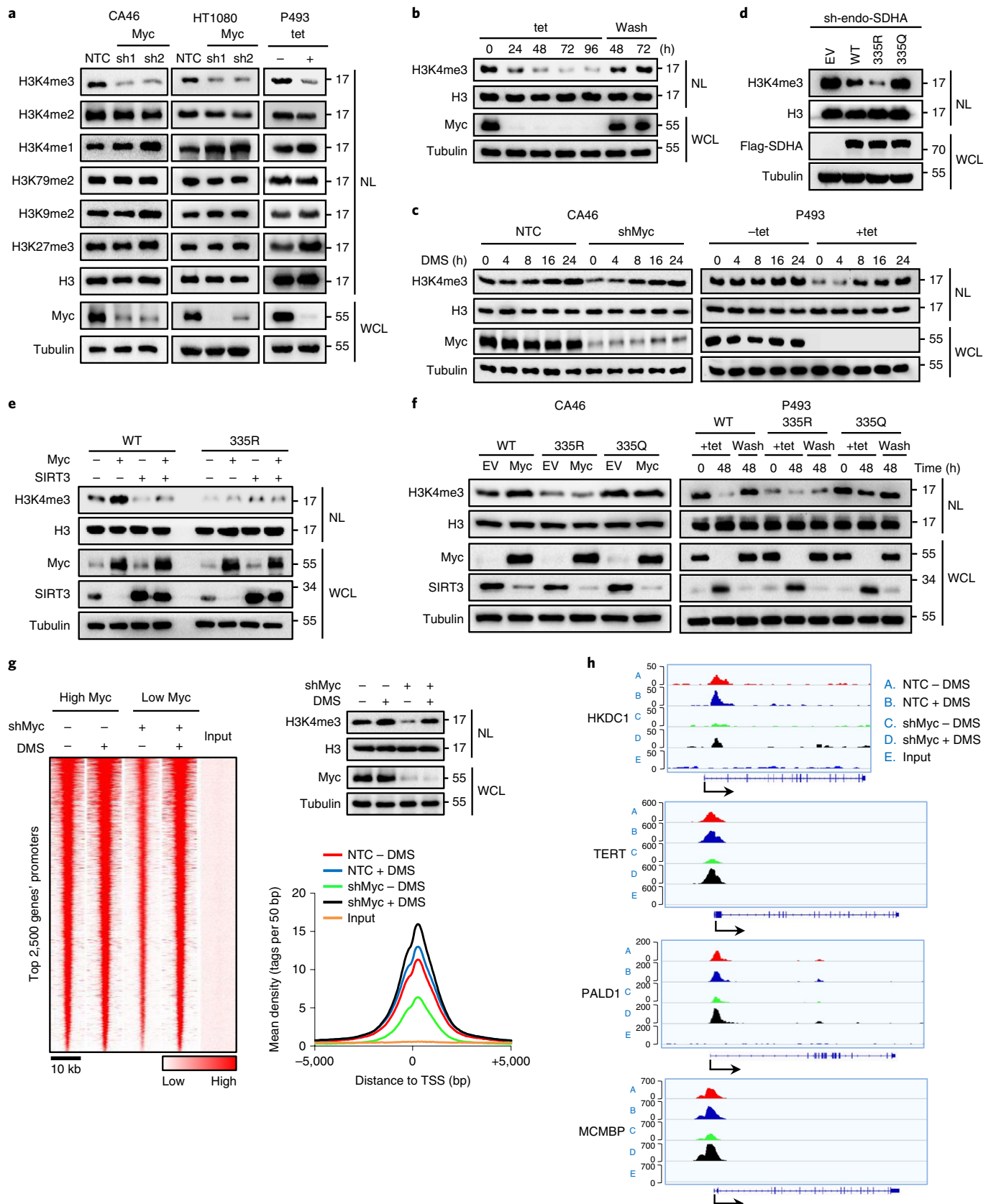
Myc enhances H3K4me3 via SDHA acetylation-mediated increase in cellular succinate. Previous reports have demonstrated that the increase in cellular succinate, which occurs in tumours deficient for SDH activity, inhibits JHDMs, resulting in epigenetic reprogramming, such as histone hypermethylation^{27,29,30,36}. Because we observed that Myc represses SDH-complex activity and consequently elevates the cellular succinate/ α -KG ratio by inducing SDHA acetylation, we next sought to explore whether Myc-accumulated succinate regulates the homeostasis of histone methylation. Interestingly, among the histone methylation modifications that we tested, H3K4me3 was dramatically reduced after suppression of Myc in different cancer-cell lines (Fig. 3a and Extended Data Fig. 3a). Moreover, the H3K4me3 levels were recovered after removing tetracycline by washing to allow re-expression in P493 cells (Fig. 3b). To investigate whether Myc modulates H3K4me3 by altering succinate levels, dimethyl succinate (DMS), a membrane-permeable succinate analogue, was introduced to treat CA46 or P493 cells with high or depleted Myc expression. As a result, DMS treatment exhibited a marginal effect on H3K4me3 in high Myc-expressing cells, whereas it significantly induced

H3K4me3 in Myc-depleted cells in a time-dependent manner (Fig. 3c), demonstrating that supplementation of succinate recovered H3K4me3 levels suppressed by Myc depletion. To further confirm whether Myc-mediated H3K4me3 changes are caused by succinate/ α -KG ratio, we performed additional experiments to treat P493 cells with dimethyl- α -KG (cell-permeable α -KG). As a result, dimethyl- α -KG treatment significantly decreased Myc-induced H3K4me3 levels (Extended Data Fig. 3b,c). More interestingly, dimethyl- α -KG could attenuate DMS-induced H3K4me3 level in Myc-depleted P493 cells (Extended Data Fig. 3c). In contrast, knockdown of SIRT3 increased the H3K4me3 levels, but not the levels of the other histone-methylation modifications we tested (Extended Data Fig. 3d). Our results also showed that overexpression of SIRT3 abolished Myc-enhanced H3K4me3 levels, whereas knockdown of SIRT3 or treatment with NAM recovered shMyc-suppressed H3K4me3 in HT1080 cells (Extended Data Fig. 3e,f), suggesting that SIRT3 is involved in Myc-regulated H3K4me3 modification. Furthermore, restoring the expression of wild-type SDHA or its K335R mutant (active form) inhibited H3K4me3 levels with endogenous SDHA knockdown (Fig. 3d). However, forced expression of the K335Q mutant (inactive form) showed no effect on H3K4me3 modification, and these cells displayed H3K4me3 levels similar to those in the empty-vector group (Fig. 3d). These findings suggest that SDHA Lys 335 acetylation suppresses H3K4me3 modification. We further found that, with restored expression of wild-type SDHA in the endogenous SDHA knockdown HT1080 cells, Myc enhanced H3K4me3 modification via SIRT3 (Fig. 3e and Extended Data Fig. 3g). However, in HT1080 cells with restored expression of SDHA K335R, which possessed less cellular succinate (Fig. 1j), H3K4me3 modification remained at a steady-state low level and was not affected by Myc (Fig. 3e). In contrast, in HT1080 cells with restored SDHA-K335Q-mutant expression, which showed more cellular succinate accumulation (Fig. 1j), H3K4me3 modification remained at high levels and was not affected by Myc (Extended Data Fig. 3g). Similar results were also observed in CA46 and P493 cells (Fig. 3f), demonstrating that SDHA Lys 335 acetylation is involved in Myc-promoted H3K4me3 modification. It has been reported that the KDM5 family of histone demethylases enzymes (including KDM5A, KDM5B, KDM5C and KDM5D) regulates H3K4me3 level³⁷. We thus measured the activities of each of the KDM5 family members and found that KDM5A activity was most significantly decreased upon succinate incubation, as compared with the activity of other KDMs in vitro (Extended Data Fig. 3h), which indicates that KDM5A

Fig. 3 | Myc enhances H3K4me3 via SDHA acetylation-mediated increase in cellular succinate. **a**, Western blot analysis of the indicated histone methylation markers and Myc in CA46 or HT1080 cells infected with viruses for expression of NTC or Myc shRNAs (sh1, sh2), or in P493 cells treated with or without tetracycline for 48 h. **b**, Western blot analysis of H3K4me3 and Myc from nuclear lysates and whole-cell lysates in P493 cells treated with tetracycline for the indicated number of hours or with washing to remove the tetracycline, followed by culturing for the indicated number of hours. **c**, CA46 cells infected with viruses for expression of NTC or Myc shRNA or P493 cells treated with or without tetracycline were exposed to 10 mM dimethyl succinate (DMS) for the indicated number of hours, followed by western blot analysis of H3K4me3 and Myc from nuclear lysates and whole-cell lysates. **d**, HT1080 cells with stable knockdown of endogenous SDHA via shRNA targeting the SDHA 3'-untranslated region (3'-UTR) were subsequently infected with viruses for expression of empty vector, Flag-wild-type-SDHA, Flag-SDHA-K335R or Flag-SDHA-K335Q, followed by western blot analysis of Flag-SDHA and H3K4me3. **e**, HT1080 cells with stable knockdown of endogenous SDHA were infected with viruses for expression of Flag-wild-type-SDHA or Flag-SDHA-K335R, followed by further infection with viruses of empty vector, or SIRT3 and empty vector or Myc. Western blot analysis of H3K4me3, Myc and SIRT3 levels. **f**, CA46 or P493 cells with stable knockdown of endogenous SDHA were infected with viruses for expression of Flag-wild-type-SDHA, Flag-SDHA-K335R or Flag-SDHA-K335Q, followed by treatment with tetracycline for the indicated number of hours or washing to remove tetracycline for 48 h or infection with viruses for expression of EV or Myc, respectively. Western blot analysis of H3K4me3, Myc and SIRT3 levels. **g**, CA46 cells infected with viruses for expression of NTC or shMyc were cultured in the presence of vehicle or 10 mM DMS for 24 h, followed by western blot analysis of H3K4me3 (top right) and ChIP-seq analysis of H3K4me3 around gene TSS regions. Heat map showing H3K4me3 levels in TSS regions for the top 2,500 gene promoters (left). Distribution analysis of H3K4me3 tags around the TSS regions of the top 2,500 genes (bottom right). $n=3$ independent experiments for western blot (top right) were repeated with similar results. One replicate ($n=1$, each group) was used for ChIP-seq assay of CA46 cells. **h**, H3K4me3 markers of ChIP-sequencing traces for the indicated genes in CA46 cells were determined by IGV software analysis. For IGV analysis, 1 replicate ($n=1$, each group) was used for H3K4me3 analysis in ChIP-seq assay of CA46 cells. $n=3$ independent experiments were repeated with similar results (**a–f**). H3 and tubulin served as loading controls. WCL, whole-cell lysates; NL, nuclear lysates. See also Extended Data Fig. 3.

is potentially responsible for Myc-mediated H3K4me3 regulation. Furthermore, we confirmed that knockdown of KDM5A blocked the inhibitory effect of Myc-depletion on H3K4me3 levels (Extended Data Fig. 3i).

To investigate Myc regulation on global gene H3K4me3 modification, we performed chromatin-immunoprecipitation sequencing (ChIP-seq) assays in Myc-expressing or Myc-depleted CA46 or P493 cells with or without DMS treatment. The H3K4me3 levels were



confirmed by western blot in CA46 and P493 cells (Fig. 3g, top right, and Extended Data Fig. 3j, top right). ChIP-seq analysis showed that H3K4me3 in the promoter regions of the top 2,500 genes was significantly suppressed by depleting Myc, which was recovered significantly by supplementation with DMS (Fig. 3g, left, and Extended Data Fig. 3j, left). A similar result was observed in analysis of the distribution of H3K4me3 tags around the TSS of 2,500 gene promoter regions (Fig. 3g, bottom right, and Extended Data Fig. 3j, bottom right). IGV analysis revealed that H3K4me3 levels in promoter regions of the *HKDC1*, *TERT*, *PALD1* and *MCMBP* genes were markedly reduced in both cell lines by suppressing Myc, and they were partially rescued by DMS treatment (Fig. 3h and Extended Data Fig. 3k). Independent ChIP assay results using H3K4me3 antibody also verified the ChIP-seq data in CA46 and P493 cells (Extended Data Fig. 3l). Taken together, these data indicate that SDHA Lys 335 acetylation and subsequent cellular succinate alterations are critical for Myc-regulated H3K4me3 modification.

Myc-mediated succinate accumulation and H3K4me3 activation promote its target gene expression. To further study whether Myc-regulated H3K4me3 affects gene expression, we performed RNA-seq analysis (RNA-seq) in Myc-expressing or Myc-depleted CA46 or P493 cells with or without DMS treatment (Extended Data Fig. 4a,b). Our results showed that depletion of Myc decreased the expression of many genes in CA46 and P493 cells, and this effect was markedly recovered by supplementation with DMS (Fig. 4a and Extended Data Fig. 4c). A more detailed analysis showed that mRNA expression of 2,162 genes was recovered with DMS in the RNA-seq data, and promoter H3K4me3 modifications of 2,500 genes were enhanced by DMS treatment in the ChIP-seq data in CA46 cells (Fig. 4b). Among them, 499 genes overlapped, showing simultaneous recovery of their mRNA as well as H3K4me3 modification by DMS treatment, which accounted for 23.1% of the DMS-regulated genes from RNA-seq and 20.0% of the DMS-regulated genes from ChIP-seq (Fig. 4b). Gene ontology (GO) term enrichment analysis further demonstrated that 499 overlapping genes were mainly involved in regulating cell metabolism (Fig. 4c). The similar RNA-seq results were also found in P493 cells (Extended Data Fig. 4d,e). Thus, we focused on the metabolic genes among those overlapping genes in CA46 and P493 cells. A ChIP assay experiment confirmed that DMS treatment recovered the Myc-depletion-suppressed H3K4me3 in the promoter regions of these metabolic genes (Extended Data Figs. 3l and 4f,g). Intriguingly, our results showed that incubation with SDHA inhibitor 3-nitropropionic acid (3-NPA) recovered Myc-depletion-suppressed H3K4me3 levels in P493 cells (Extended Data Fig. 4h). More importantly, RNA-seq and ChIP analysis revealed that treatment with 3-NPA recovered Myc-depletion-suppressed gene expression as well as H3K4me3 modification of gene promoter regions (Extended Data Fig. 4i,j).

Furthermore, Myc depletion drastically inhibited the expression of these metabolic genes at both the mRNA and protein levels, which was partially rescued by DMS supplementation (Fig. 4d,e and Extended Data Fig. 4k,l). Notably, we found that, in CA46 or P493 cells with endogenous SDHA knockdown, with restored expression of wild-type SDHA, Myc drastically enhanced the mRNA and protein expression of these metabolic genes (Fig. 4f,g and Extended Data Fig. 4m,n). However, in cells with restored expression of SDHA-K335R, both the mRNA and protein expression of these metabolic genes remained very low (Fig. 4f,g and Extended Data Fig. 4m,n), which is consistent with the H3K4me3 data in Fig. 3f. Collectively, our data demonstrate that Myc-mediated succinate accumulation and H3K4me3 activation promote its target gene expression.

SDHA acetylation at Lys 335 contributes to Myc-promoted tumour progression. A loss-of-function mutation in SDHA contributes to tumour progression in multiple types of cancers^{21,25,26}. Thus, it is of

interest to investigate the effect of SDHA Lys 335 acetylation, which also results in its deactivation, on tumour-cell proliferation. To address this issue, we used HT1080 or P493 cells stably expressing shSDHA to suppress the expression of endogenous SDHA, in which shRNA-resistant wild-type SDHA wild-type, of the K335R (non-acetylation mimic) or K335Q (acetylation mimic) mutants, was further restored. Intriguingly, the K335R mutant impaired, while the K335Q mutant promoted, cell proliferation compared with that in the SDHA wild-type group in HT1080 cells (Fig. 5a). Moreover, when Myc was overexpressed in HT1080 cells, the K335Q mutant exhibited an effect similar to that of wild-type SDHA on cell proliferation, while the K335R mutant still strongly inhibited cell proliferation (Fig. 5a). Similar results were also observed in P493 cells with high Myc expression (Extended Data Fig. 5a), indicating that Myc-induced highly acetylated SDHA had a similar effect of the K335Q mutant on promoting cell proliferation. Furthermore, treatment of HT1080 cells with dimethyl- α -KG³⁸ diminished the stimulating effect of the K335Q mutant on cell proliferation (Extended Data Fig. 5b), suggesting that the succinate/ α -KG ratio is critical for the effect of SDHA acetylation on Myc-mediated cancer-cell proliferation. After demonstrating that KDM5A is critical for Myc-mediated H3K4me3 regulation (Extended Data Fig. 3h,i), we next explored whether KDM5 activity was involved in modulating the effect of Myc-mediated SDHA Lys 335 acetylation on tumour-cell proliferation. Intriguingly, we found that treatment with KDM5 inhibitor CPI-455 (ref. ³⁹) diminished the inhibitory effect of K335R mutant on cell proliferation in HT1080 cells (Extended Data Fig. 5c), indicating that KDM5 activity is involved in modulating the effect of Myc-mediated SDHA Lys 335 acetylation on tumour cell proliferation.

Consistent with the cell-growth data, mouse xenograft experiments using the same HT1080 cells as in Fig. 5a revealed that the K335R mutant slowed, while the K335Q promoted, tumour growth compared with that with wild-type SDHA. In Myc-overexpressing HT1080 xenograft tumours, the K335Q mutant exhibited an effect similar to that of wild-type SDHA on tumour growth, while the K335R mutant still displayed a significant inhibitory effect on tumour growth in vivo (Fig. 5b,c and Extended Data Fig. 5d). Moreover, succinate or α -KG measurement using tumour tissue lysates showed that restoring the expression of the K335R mutant led to a significant reduction of succinate level and succinate/ α -KG ratio, while the K335Q mutant showed markedly increased succinate level and succinate/ α -KG ratio compared with those with wild-type SDHA. More importantly, when Myc was overexpressed, tumours expressing the K335Q mutant exhibited a similar succinate level and a succinate/ α -KG ratio as tumours expressing wild-type SDHA, while cellular succinate level and succinate/ α -KG ratio in tumours expressing K335R mutant remained at low levels (Fig. 5d and Extended Data Fig. 5e,f). Western blot analysis confirmed the regulatory effect of Myc on SIRT3 as well as the K335-acetylated SDHA and H3K4me3 levels in different tumour groups (Fig. 5e). To further explore whether α -KG affects in vivo tumour growth by modulating Myc-mediated SDHA Lys 335 acetylation, we performed mouse xenograft experiments using the same HT1080 cells as in Extended Data Fig. 5b using nude mice, which were treated with PBS or 0.6 g per kg (body weight) dimethyl α -KG. As a result, dimethyl- α -KG diminished the stimulating effect of the K335Q mutant on tumour growth, demonstrating that succinate/ α -KG ratio is critical for the effect of SDHA acetylation on Myc-mediated tumour growth (Extended Data Fig. 5g,h). Western blot analysis confirmed that H3K4me3 levels were suppressed by dimethyl- α -KG in mouse xenograft tumour tissues (Extended Data Fig. 5i). Meanwhile, we also carried out mouse xenograft experiments using the same HT1080 cells as in Extended Data Fig. 5c. The nude mice were treated with vehicle or 20 mg per kg KDM5 inhibitor CPI-455 to test the effect of KDM5 activity on tumour growth. Consistent with the in vitro cell-growth data, treatment with KDM5 inhibitor CPI-455 diminished the inhibitory effect

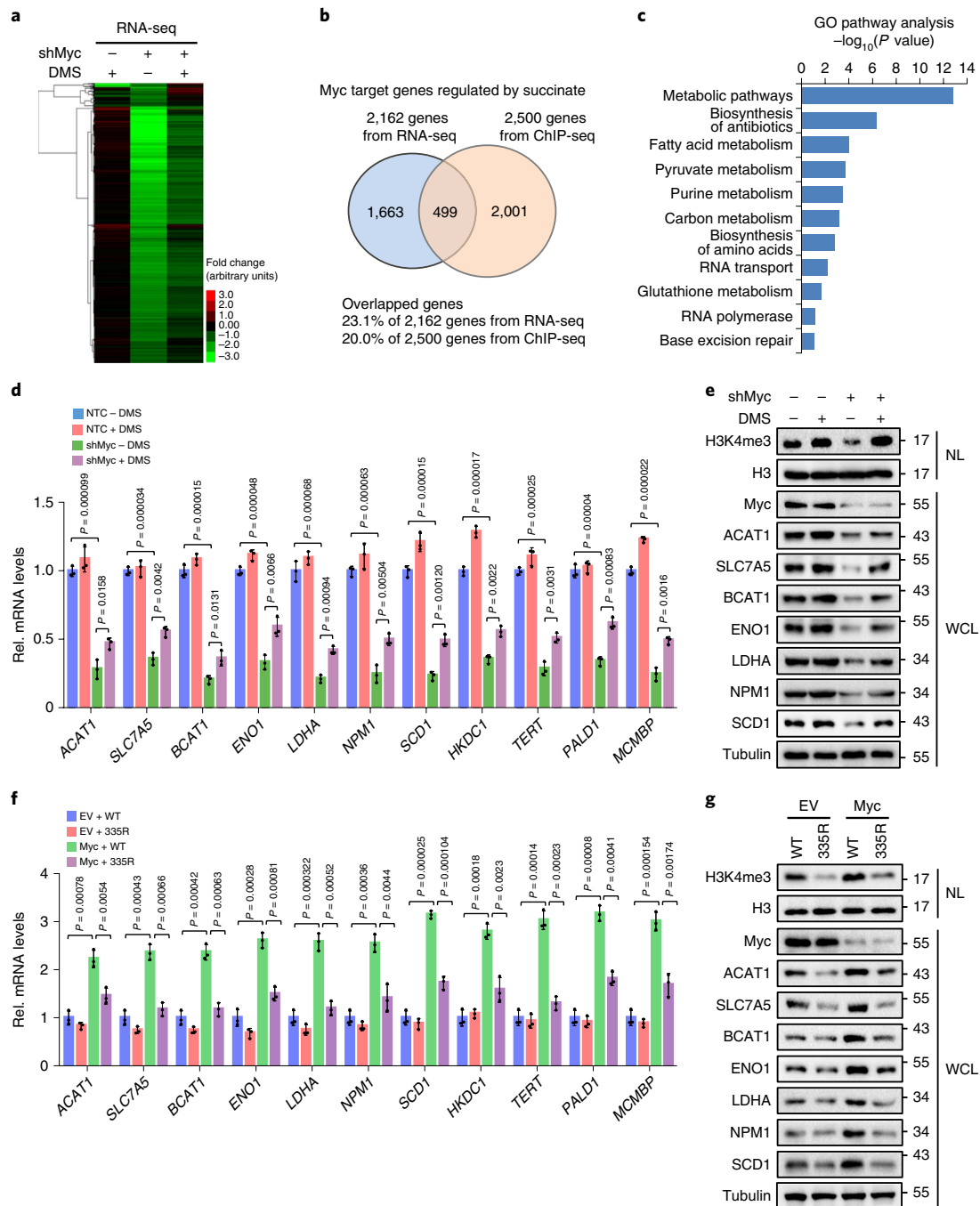


Fig. 4 | Myc-mediated succinate accumulation and H3K4me3 activation promote its target gene expression. **a**, Heat map of the RNA-seq results showing that the genes with downregulated expression following Myc depletion were subsequently rescued by DMS treatment in CA46 cells (fold change > 1.5). The statistical significance between Myc- and succinate-regulated genes was determined using two-sided Fisher's exact probability, $P < 0.001$. The sufficient RNA-seq samples ($n=1$, each group) used to analyse the heat map and statistics. **b**, Venn diagram showing overlapping genes co-regulated by Myc and succinate based on the RNA-seq data and ChIP-seq data in CA46 cells. Correlation significance between genes with mRNA levels and genes with H3K4me3 that were rescued by DMS based on RNA-seq and ChIP-seq, respectively, were determined using the two-sided Spearman test, $P < 0.001$. **c**, Analysis of 499 overlapping genes by Gene Ontology (GO) term enrichment. Group differences are analysed by the two-tailed Student's t test. The sufficient RNA-seq samples ($n=1$, each group) were analysed in GO term enrichment. **d**, The mRNA levels of the indicated genes were determined by quantitative real-time PCR (qRT-PCR) in the CA46 cells used in **a**. Data are presented as the mean \pm s.d. of 3 independent experiments ($n=3$). Group differences are analysed by the two-tailed Student's t test. $P < 0.05$ compared with the NTC-DMS group; $P < 0.05$ compared with the shMyc-DMS group. **e**, The indicated proteins were assessed by western blotting in the CA46 cells used in **d**. **f**, CA46 cells with endogenous SDHA knockdown were further constructed to stably express Flag-wild-type-SDHA or Flag-SDHA-K335R, followed by infection with viruses for expression of EV or Myc. The mRNA levels of the indicated genes were determined by qRT-PCR. Data are presented as the mean \pm s.d. of three independent experiments ($n=3$). Group differences are analysed by the two-tailed Student's t test. $P < 0.05$ compared with the EV + WT group; $P < 0.05$ compared with the Myc + WT group. **g**, The indicated protein levels were determined by western blotting in the CA46 cells used in **f**. $n=3$ independent experiments were repeated with similar results (**e,g**). Tubulin and H3 served as loading controls. Data are presented as the mean \pm s.d. of three independent qRT-PCR experiments. See also Extended Data Fig. 4.

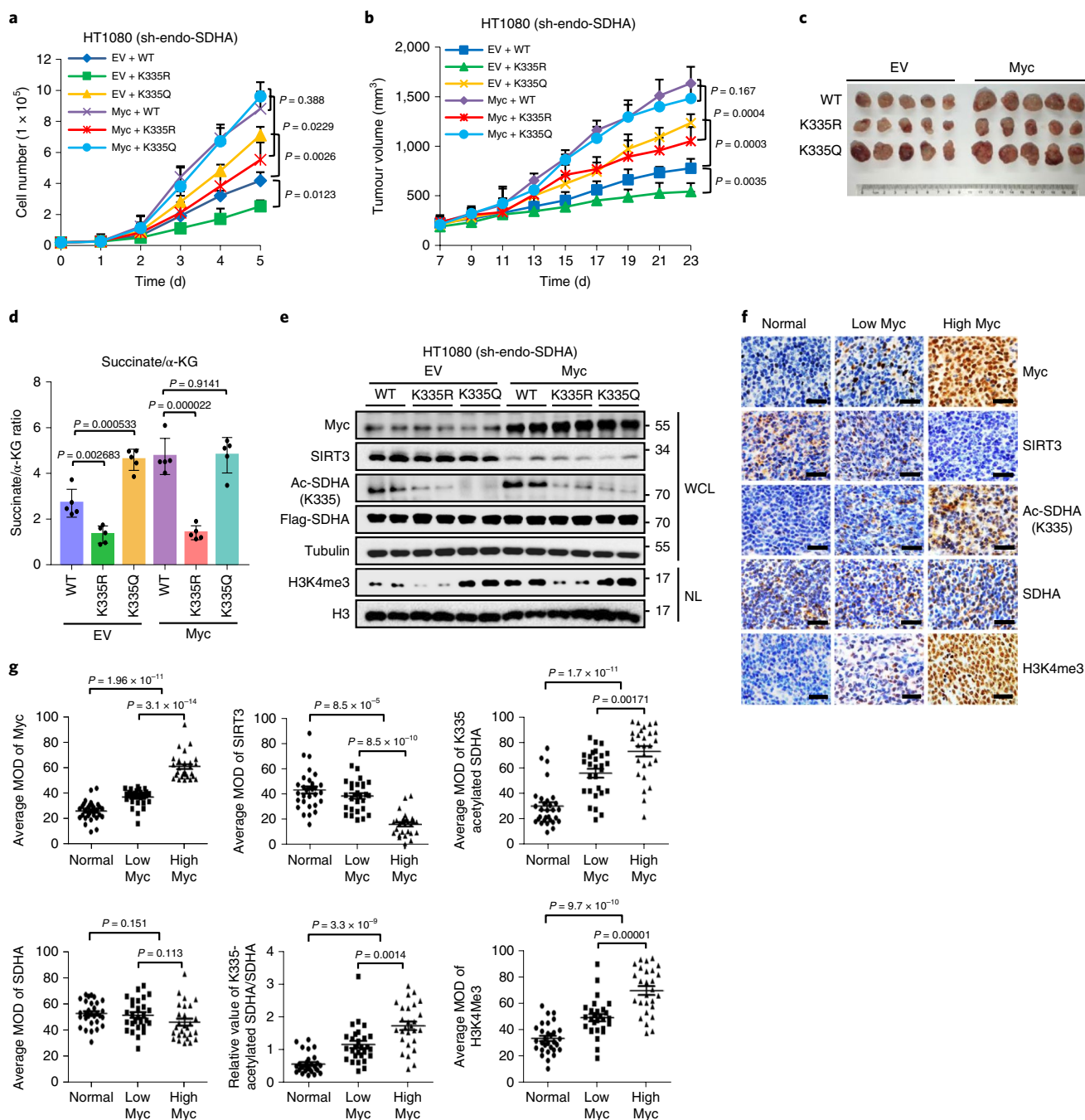


Fig. 5 | SDHA acetylation at Lys 335 contributes to Myc-promoted tumour progression. **a**, HT1080 cells with endogenous SDHA knockdown and further expressing Flag-wild-type-SDHA, Flag-SDHA-K335R or Flag-SDHA-K335Q, were infected with viruses for expression of pMX-GFP empty vector or pMX-GFP-Myc. The growth of HT1080 cells was determined by trypan blue staining. Data are presented as the mean \pm s.d. ($n = 3$, each group). Group differences are analysed by the two-tailed Student's *t* test. $P < 0.05$ compared with the indicated group. **b,c**, HT1080 cells used in **a** were injected subcutaneously into BALB/c nude mice ($n = 5$, each group). Tumour growth curves were measured starting 7 d after inoculation (**b**). Tumours were extracted and compared at the end of the experiment (**c**). Group differences are analysed by the two-tailed Student's *t* test. $P < 0.05$ compared with the indicated group. **d**, The succinate and α -KG levels were measured with assay kits using cell lysates from xenograft tumour tissues ($n = 5$, each group), then succinate/ α -KG ratio was calculated. The succinate and α -KG levels were normalized to cellular protein levels. Group differences are analysed by the two-tailed Student's *t* test. $P < 0.05$ compared between indicated groups. **e**, Levels of Myc, SIRT3, SDHA and Lys 335 acetylation of SDHA and H3K4me3 were determined by western blot using the nuclear lysates and whole-cell lysates of tumour tissues from each group, as in **c**. Tubulin and H3 served as loading controls. $n = 5$ independent xenograft tumour tissue lysates in each group were repeated by western blot, with similar results. **f**, Example images are shown. Representative IHC analysis of Myc, SIRT3, SDHA, Lys 335 acetylation of SDHA and H3K4me3 in low and high Myc-expressing DLBCL samples and normal tissues. The scale bar is 20 μm in each image. The clinical DLBCL lesions ($n = 55$) and normal lymph-node samples ($n = 30$) were used for Immunohistochemistry (IHC). **g**, Statistical analysis of all samples shown in **f**. The intensities of the indicated proteins were quantified using the HistoQuest software. Statistical analysis of indicated protein quantification in clinical DLBCL lesions ($n = 55$) and normal lymph-node ($n = 30$) samples. Data are presented as the mean \pm s.e.m. Group differences are analysed by the two-tailed Student's *t* test. $P < 0.05$ compared with the corresponding control group. See also Extended Data Fig. 5.

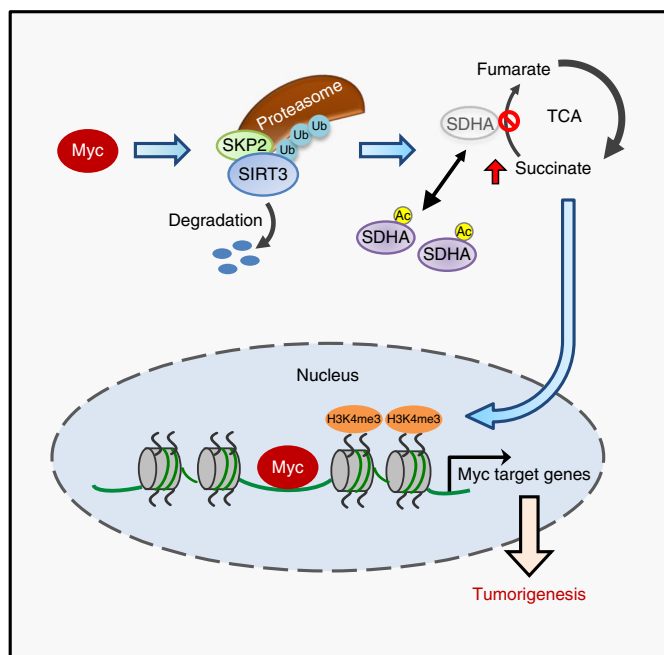


Fig. 6 | Myc-mediated SDHA acetylation and H3K4me3 activation trigger epigenetic regulation of gene expression and tumorigenesis. Schematic showing that high Myc expression facilitates acetylation-dependent deactivation of SDHA by activating SKP2-mediated degradation of SIRT3 deacetylase. Consequently, inhibition of SDHA activity leads to cellular succinate accumulation, which triggers H3K4me3-mediated tumour-specific gene expression and cancer progression.

of K335R mutant on tumour growth in HT1080 cells (Extended Data Fig. 5j,k). Western blot revealed that CPI-455 elevated H3K4me3 levels in mouse xenograft tumour tissues (Extended Data Fig. 5l).

To further study the physiological relevance and potential clinical relevance of this regulatory pathway, immunohistochemistry (IHC) was performed using 55 clinical diffuse large B cell lymphoma (DLBCL) lesions and 30 normal lymph-node samples. DLBCL is the most common type of non-Hodgkin's lymphoma (NHL) and is highly invasive and malignant. Myc is highly expressed and translocated to the nucleus, which increases tumour malignancy and results in a poor prognosis in many DLBCLs^{40–44}. As expected, DLBCLs displayed elevated Myc staining compared with that in normal lymph nodes (Fig. 5f,g). We further analysed the mean optical density (MOD) of Myc staining for all clinical samples using HistoQuest software. A MOD cutoff of $\geq 50\%$ was used to define high Myc expression, as previously reported^{40,45}. Thus, the 55 DLBCL samples were divided into two groups, one with high Myc expression (27 samples with MOD of Myc staining $\geq 50\%$) and the other group with relatively low Myc expression (28 samples with MOD of Myc staining $< 50\%$), for further analysis. IHC staining revealed that SIRT3 protein was negatively, but Lys 335-acetylated SDHA and H3K4me3 were positively, correlated with Myc expression (Fig. 5f). Quantification of the images using HistoQuest software further provided statistical results showing that Myc expression was negatively correlated with SIRT3 protein ($P < 0.0001$) but positively correlated with Lys 335-acetylated SDHA and H3K4me3 levels ($P < 0.0001$) in DLBCLs (Fig. 5g). Thus, our clinical data revealed that Lys 335 acetylation of SDHA might potentially represent a promising biomarker for DLBCLs.

Discussion

It is well established that Myc regulates the expression of many genes by binding to E-boxes and recruiting histone acetyltransferases⁴⁶.

However, it is unclear how Myc-mediated epigenetic modification is involved in this process. Although several reports suggest a potential regulatory correlation between Myc and H3K4me3 (refs. ^{8,14}), evidence is still lacking concerning whether and how Myc modulates H3K4me3 levels in human cancer cells. In this study, we demonstrated that H3K4me3 was regulated by Myc in cancer cells via a previously unappreciated mechanism. We found that Myc repressed SDH activity via acetylation to accumulate cellular succinate and activate H3K4me3. Furthermore, supplementation of dimethyl succinate partially rescued the inhibitory effect of Myc depletion on H3K4me3 levels (Fig. 3c,g,h). More interestingly, RNA-seq analysis provided supportive results showing that Myc was involved in H3K4me3-mediated gene expression (Fig. 4). Collectively, we here reveal a mechanism in which Myc-facilitated H3K4me3 modification is critically involved in the epigenetic regulation of gene expression in cancer cells.

There is now growing recognition of the essential roles of lysine acetylation in metabolism. Recent studies have revealed advances in the regulation of the acetylation of metabolic enzymes involved in cancer-cell metabolic reprogramming and tumorigenesis^{47–50}; however, it is not clear how such acetylation modifications are regulated in cancer cells. Here, we revealed that Myc, which is known for its capacity to rewire metabolic pathways by controlling gene expression^{6,51}, can widely affect lysine acetylation of mitochondrial proteins in human cancer cells by accelerating SKP2-mediated proteasomal degradation of SIRT3. By using a screening approach to determine changes in lysine acetylation in enzymes influenced by Myc, we found that the acetylation of SDHA was closely correlated with Myc expression (Fig. 1c,d and Supplementary Table 1). We demonstrated that Myc increased the acetylation of SDHA at Lys 335 to inhibit SDH-complex activity (Fig. 1), leading to succinate accumulation and succinate/ α -KG ratio elevation (Fig. 1i,j and Extended Data Fig. 1m–o). Our results reveal a link between oncogenic Myc and tumour-suppressor SDHA, whereby Myc controls the metabolic switch by regulating acetylation-mediated enzyme activity in tumour cells.

The contribution of Myc-driven SDHA acetylation at Lys 335 to cancer progression both in vitro and in vivo is very intriguing. We showed that the K335R mutant (non-acetylation mimic) suppressed, while the K335Q mutant (acetylation mimic) facilitated, cell proliferation compared with what occurred in the SDHA wild-type group in HT1080 cells or xenograft tumours. Furthermore, in Myc-overexpressing HT1080 cells or xenograft tumours, the K335Q mutant exhibited an effect similar to the wild-type SDHA on cell proliferation, while the K335R mutant still strongly inhibited cell proliferation (Fig. 5a–c). Of note, we also discovered that SDHA-K335R mutation did not completely block the effect of overexpressed Myc on cell proliferation. This indicates that Myc may also regulate tumour proliferation by other mechanisms, as documented by many previous studies^{51–53}.

More importantly, IHC staining of 55 clinical DLBCL and normal lymph-node samples showed that SIRT3 protein gradually declined while Lys 335-acetylated SDHA and H3K4me3 levels gradually increased in normal lymph-node samples in low-Myc-expression DLBCL and high-Myc-expression DLBCL, respectively (Fig. 5f,g). These results suggested that SIRT3 might have a tumour-suppressor function, while Lys 335-acetylated SDHA might promote tumour progression in DLBCLs with high Myc expression. On the basis of these results, we propose that Myc inhibits SIRT3 to increase Lys 335-acetylated SDHA levels, inhibiting SDH-complex activity to accumulate succinate, which promotes H3K4me3 activation and tumour-specific gene expression (Fig. 6). This finding is highly relevant for understanding the pathogenic role of SDHA acetylation during Myc-dysregulated cancer progression. Although SDHA is recognized as a tumour suppressor and its loss-of-function mutant is sparsely associated with various tumours, such as pheochromocytoma, paraganglioma, breast cancer and renal-cell carcinoma, among others^{23,25,26,36,54,55}, it is not clear to date whether other means

exists to regulate SDH function during cancer progression. Hence, the tumorigenic role following its loss of function might have been underestimated. For example, one recent report showed that only ~3% of people with breast cancer harbour an SDHA mutation²⁶. In contrast, we provide evidence herein suggesting that, at least for DLBCL, SDHA loss of function via acetylation contributes much more broadly to tumour progression in which Myc is deregulated (Fig. 5f,g), suggesting a potential rationale to target the acetylation of SDHA in general for Myc-deregulated DLBCL therapy.

Methods

Cell cultures and reagents. HEK293T (from ATCC) and HT1080 (from Chinese Academy of Sciences, Shanghai) cells were cultured in DMEM (GIBCO). The human P493-6 B cell line (a gift from C. V. Dang) containing a tetracycline-repressible Myc system²⁶, CA46 cells (from Cobiaer), Raji cells (from Chinese Academy of Sciences) were maintained in RPMI 1640 (GIBCO). The routine media were supplemented with 10% FBS and 1% penicillin–streptomycin, while CA46 cells' media were supplemented with 20% FBS and 1% penicillin–streptomycin. The cells were cultured at 37°C in a humidified atmosphere with 5% CO₂ in air. Trypan blue exclusion was used to assess cell growth. Nicotinamide (NAM, N0636), trichostatin A (TSA, V900931), MG132 (C2211) and dimethyl succinate (73605) were purchased from Sigma-Aldrich. Lactacystin (2267) was purchased from TOCRIS.

Plasmids and establishment of stable cell lines. The pMX-GFP-Myc vector was a gift from C. V. Dang. All shRNAs in the PLKO vector against Myc, SKP2 or SIRT3 were commercially purchased (Sigma-Aldrich). shRNAs targeting the SDHA 3'-UTR were constructed in the PLKO vector. SIRT3 was subcloned into the pSIN-EF2 vector with a 3×Flag tag at the carboxy-terminus or without a tag. SKP2 was also subcloned into the pSIN-EF2 vector with a V5 tag or 3×Flag tag. KDM5A, KDM5B, KDM5C and KDM5D were subcloned into the pSIN-EF2 vector with a 3×Flag tag. SDHA was subcloned into the PQCXIN vector with a 3×Flag tag at the C-terminus. The shRNA targeting sequences are listed in Supplementary Table 3. Briefly, HT1080 cells, CA46 cells or P493 cells were infected with retrovirus (Myc or SDHA) or lentivirus (SIRT3 or all shRNAs) in the presence of polybrene, followed by selection with 0.4 µg ml⁻¹ of puromycin or 0.8 mg ml⁻¹ of G418 to establish stable cells.

Sample preparation for mitochondrial protein. Mitochondrial protein lysates for LC–MS/MS were extracted from cells as previously described^{17,57}. Briefly, cells were collected and homogenized in ice-cold mitochondrial isolation buffer (10 mM KCl, 1.5 mM MgCl₂, 10 mM Tris–Cl (pH 7.4), 5 µM trichostatin A, 50 mM nicotinamide) supplemented with protease inhibitor cocktail (Roche). Unbroken cells and nuclei were pelleted by centrifugation at 1,200g for 10 min at 4°C. Then, the supernatants were centrifuged at 4,000g for 20 min at 4°C to remove lysosome and endoplasmic reticulum and pellet the mitochondria. The pellets were washed with isolation buffer and further centrifuged at 10,000g for 15 min at 4°C, and the pellets were lysed in mitochondria lysis buffer supplemented with deacetylase inhibitors for 1 h. The mitochondria lysates were centrifuged at 12,000 r.p.m. for 10 min, and the supernatants containing the mitochondrial proteins were collected.

Protein digestion. The mitochondrial extraction was reduced and alkylated with 3 mM tris (2-carboxyl) phosphine (TCEP) and 20 mM iodoacetamide (IAM) at 37°C in darkness. Protein precipitation was performed afterward by stepwise addition of 6 volumes of ice-cold acetone, followed by centrifugation at 22,000g for 10 min, and then the resulting pellet was rinsed twice with cold acetone to remove residual salts, re-suspended in 50 mM NH₄HCO₃ (pH 8.2) and digested with trypsin or chymotrypsin. Digestion was terminated by addition of 1 µl formic acid (FA), followed by centrifugation at 20,000g at 4°C for 10 min. The supernatants were dried in a SpeedVac.

Affinity purification of lysine-acetylated peptides. The affinity-purified anti-acetyl lysine antibody (Cell Signaling Technology) was immobilized onto protein A/G-conjugated agarose beads at 3–4 mg ml⁻¹ by incubation at 4°C for 4 h. The supernatant was removed, and the beads were washed three times with NETN buffer (50 mM Tris–HCl pH 8.0, 100 mM NaCl, 1 mM EDTA, 0.5% NP40). The peptides obtained from the above conditions were resolubilized in NETN buffer. Insoluble particles were removed by centrifugation at 100,000g for 10 min. Affinity purification was carried out by incubating the peptides with 20 ml of anti-acetyl lysine antibody-immobilized protein A/G-conjugated agarose beads at 4°C for 6 h with gentle shaking. The beads were washed three times with 1 ml of NETN buffer and twice with ETN buffer (50 mM Tris–HCl pH 8.0, 100 mM NaCl, 1 mM EDTA). Bound peptides were eluted from the beads three times with 50 ml of 0.1% TFA. The eluted peptides were combined and dried in a SpeedVac. The resulting peptides were cleaned in mC18 ZipTips (Millipore) according to the manufacturer's instructions, prior to nano LC–MS/MS analysis.

Nano LC–MS/MS configuration. Proteolytic peptides were reconstituted with mobile phase A (2% acetonitrile containing 0.1% formic acid) and then separated on a nano-LC column (75 µm ID × 10 cm, packed with Pepmap 3 µm C18 material). Mobile phase A consisted of 0.1% formic acid in 2% acetonitrile, and mobile phase B was 0.1% formic acid in 84% acetonitrile. A linear gradient from 3 to 100% B over 75 min at a flow rate of 350 nl min⁻¹ was applied. Mass spectrometry analysis was carried out on a Q-Exactive mass spectrometer (Thermo Fisher) operated in data-dependent scan mode. Survey scan (*m/z* 375–1,300) was performed at a resolution of 60,000, followed by MS2 scans to fragment the 50 most abundant precursors with collision-induced dissociation. The activation time was set at 30 ms, the isolation width was 1.5 AMU, the normalized activation energy was 35% and the activation *q* value, a setting of field radio frequency, was 0.25.

Mass spectrometry data analysis. The mass spectrometry raw file was searched by Proteome Discovery version 1.3 using the MASCOT search engine with a percolator against the human ref-sequence protein database (updated on 4 July 2016). The mass tolerance was set at 20 ppm for the precursor and 0.2 Da for the product ion. Missed cleavages were no more than four for each peptide. Carbamidomethylation of cysteine (+57.0214) was searched as a fixed modification. Lysine acetylation (+42.0106), amino-terminal protein acetylation and methionine oxidation (+15.9949) were set up as variable modifications. Peptide spectral matches were filtered to a 1% false-discovery rate using linear discriminant analysis in combination with the target-decoy strategy. Fragment assignment of each Kac-modified peptide was subject to manual inspection and validation using the original tandem mass spectra acquired in profile mode.

Immunoprecipitation and western blot assay. For immunoprecipitation assays, briefly, cells were lysed with NP-40 buffer (20 mM Tris–HCl, pH 7.5, 150 mM NaCl, 1.5 mM MgCl₂, 2 mM EDTA, 0.5% NP-40) supplemented with protease inhibitor cocktail (Roche) for 40 min on ice. Cell lysates were incubated with primary antibodies for 4 h and then with protein A/G-Sepharose beads (Thermo). The beads were washed four times with 0.2% NP-40 buffer and further boiled in 2× SDS loading buffer before western blot analysis.

For western blot assays, cells were lysed with RIPA buffer (50 mM Tris–HCl, pH 8.0, 150 mM NaCl, 5 mM EDTA, 0.1% SDS, 1% NP-40) supplemented with protease inhibitor cocktail. To detect protein levels of methylated histone H3, the extracted nuclear fractions from cells were lysed with nuclear buffer (50 mM Tris–HCl, pH 7.5, 500 mM NaCl, 1 mM EDTA, 0.2% NP-40, 10 mM β-mercaptoethanol, 10% glycerol) supplemented with protease inhibitor cocktail, and then the nuclear lysates were sonicated using an Ultrasonic Cell Disruptor (Scientz). Equal amounts of proteins were fractionated by 5–12% SDS–polyacrylamide gel electrophoresis (SDS–PAGE). Signals were detected using Western ECL Substrate (Bio-Rad). Primary antibodies against the following proteins were used: SDHA (14865-1-AP), SKP2 (15010-1-AP), ACAT1 (16215-1-AP), ENO1 (11204-1-AP), LDHA (19987-1-AP), NPM1 (60096-1-Ig), Ubiquitin (10201-2-AP), Calreticulin (10292-1-AP), COX4 (11242-1-AP), LaminB1 (12987-1-AP), SIRT4 (21440-1-AP) and SIRT5 (15122-1-AP); KDM5C (14426-1-AP) and KDM5D (22739-1-AP) were purchased from Proteintech; Pan-acetyl-lysine (9441s), SLC7A5 (5347), KDM5A (3876S), H3K4me3 (9751S), H3K4me2 (9725), H3K4me1 (5326), H3K79me2 (5427), H3K9me2 (4658), H3K27me3 (9733) and SIRT3 (C73E3) (2627) were purchased from Cell Signaling Technology; Flag-M2 (F1804) and HA (H9658) were purchased from Sigma-Aldrich; BCAT1(3F5) (ab195663), H3 (ab1791) and V5 (ab9116-100) were purchased from Abcam; Myc (9E10) (sc40, Santa Cruz); Myc (9E10) (MA1-980, Zymed, Invitrogen); SCD (CD.E10) (NB600-1133, Novus); β-Tubulin (10B1) (M20005, Abmart); H3K4me3 (07-473, Millipore); KDM5B (A7772, Abclonal); and SDHA-K335Ac were generated by immunization of rabbits at Abclonal. A list of antibodies used in this manuscript is available in Supplementary Table 6, which includes links to manufacturer and antibody validation data.

qRT–PCR. Total RNA was isolated using TRIzol reagent (Life Technologies) followed by DNase (Ambion) treatment and reverse transcription with the iScript cDNA Synthesis Kit (Bio-Rad). qRT–PCR was performed using SYBR Green master mix (Vazyme) on a Bio-Rad iCycler. Sequences of the used primer are shown in Supplementary Table 4. All samples were normalized to 18S rRNA, and the fold change of target mRNA expression was calculated based on the threshold cycle (*C_t*), where $\Delta C_t = C_{t_{\text{target}}} - C_{t_{18S}}$ and $\Delta(\Delta C_t) = \Delta C_{t_{\text{Control}}} - \Delta C_t$.

Metabolic enzyme activity or assay. SDH activity was measured with a kit (BioVision) following the manufacturer's instructions. Briefly, whole-cell lysates or mitochondrial extracts were mixed with reagents, followed by measuring the absorbance at 600 nm using a Thermo Spectrophotometer System.

Metabolic assay. Intracellular succinate or fumarate was measured with individual kits (BioVision) following the manufacturer's instructions. The values were normalized to the protein concentration.

LC–MS analysis of metabolites. Roughly 1 × 10⁷ cells were washed twice with cold PBS, and polar metabolites were extracted by pre-cold 80% methanol immediately.

The supernatant was collected and subjected to lyophilization. The lyophilized samples were dissolved in 80% methanol to run HPLC-MS. For the kinetic LC-MS analysis, a Shimadzu NexeraX2 UHPLC combined with a Sciex 5600 Triple Time of Flight-Mass Spectrometry (TOFMS) was used, which was controlled by Sciex Analyst 1.7.1 instrument acquiring software. A Kinetex 2.6- μ m HILIC 100-Å (150 cm \times 2.1 mm, 2.6 μ m) column was used with mobile phase (A) consisting of 5 mM ammonium acetate pH 6.8; mobile phase (B) consisting of 90% acetonitrile (ACN) and 10% 50 mM ammonium acetate pH 6.8. Gradient program: mobile phase (B) was held at 100% for 5 min and then increased to 50% in 10 min and held for 2 min before returning initial condition. The column was held at 40 °C and 5 μ l of sample was injected into the LC-MS with a flow rate of 0.3 ml min⁻¹. Automatic calibrations of TOFMS were achieved with average mass accuracy of <2 ppm. Data processing software included Sciex PeakView 2.2, MasterView 1.1, and MultiQuant 3.0.2. The LC-MS measurements were normalized to cellular protein content.

Ubiquitination assay. HEK293T cells were co-transfected with pSIN-HA-ubiquitin and pSIN-Flag-SIRT3 in the presence of sh-SKP2 and pMX-Myc or V5-SKP2 and sh-Myc as indicated. After incubation for 48 h, proteasome inhibitor MG132 was added to the culture medium for an additional 8 h, followed by collection of the cells and protein lysis with SDS buffer. Equal amounts of protein lysates were immunoprecipitated with anti-Flag-M2 antibody and subjected to SDS-PAGE, followed by blotting with anti-ubiquitin antibody.

ChIP-seq and data analysis. For P493 cells, ChIP-seq assay was performed with an EZ-ChIP kit (Millipore) following the manufacturer's instructions. Briefly, for H3K4me3 ChIP, 3 \times 10⁷ cells were used. ChIP-seq was performed at the genome-sequencing company BGI, and sequencing was performed on the Illumina HiSeq2500 platform. Sequenced reads were mapped to the UCSC human genome hg19 using Bowtie2 software (version 2.2.6). For the CA46 cells' ChIP-seq experiments with spike-in control, *Drosophila* Chromatin (53083, Active Motif) and a *Drosophila*-specific antibody (61686, Active Motif) were used for each reaction. The *D. melanogaster*-specific antibody is used to immunoprecipitate *D. melanogaster* chromatin from each reaction, which is then used as a reference for normalization during data analysis. And ChIP-seq was performed at Novogene on the Illumina novaseq6000 platform. Sequenced reads were separately aligned to either the human genome hg19 or the *D. melanogaster* genome (dm6) using Bowtie2 software (version 2.2.6). The method of ChIP-seq normalization referred to the manufacturer's instruction (Active Motif). Aligned reads were used for subsequent generation of binding profiles, peak calling, motif analysis and travelling ratio analysis. Peaks were classified on the basis of the location (UCSC annotation data) and shown in the following genome regions: intergenic, introns, downstream, upstream and exons. The gene traces were visualized using the Integrative Genomics Viewer. Original data of ChIP-seq in P493 cells or CA46 cells are available in the NCBI Gene Expression Omnibus (GEO) (accession numbers GSE124255 and GSE141227, respectively).

ChIP-qPCR assay. The ChIP assay was performed with an EZ-ChIP kit (Millipore) following the manufacturer's instructions. Briefly, cells were fixed with 1% formaldehyde and quenched with 0.125 M glycine. Cells were sonicated using an Ultrasonic Cell Disruptor (Scientz). DNA was immunoprecipitated with either control IgG or H3K4me3 primary antibody. RNA and protein were digested using RNase A and Proteinase K, respectively, followed by qPCR analysis. The primers used for analysis are shown in Supplementary Table 5.

RNA-seq and data analysis. Briefly, total RNA was extracted using TRIzol Reagent following the manufacturer's instructions. RNA integrity was checked using an Agilent Bioanalyzer 2100. A total amount of 3 μ g RNA per sample was used as input material for the RNA sample preparations. Sequencing libraries were generated using the NEB Next Ultra RNA Library Prep Kit for Illumina (NEB). RNA was sequenced by Novogene using the Illumina HiSeq4000 platform. Reads were aligned to the human genome hg19 with TopHat2 v2.1.0. Gene-expression analysis was performed using Cuffdiff v2.2.1. Unsupervised clustering was performed using the cluster and tree view and visualized using heat maps. Enrichment pathway analysis of genes was compiled from GO enrichment analysis and Kyoto Encyclopedia of Genes and Genomes (KEGG) pathway databases by DAVID Bioinformatics Resources. Original data of RNA-seq in P493 or CA46 cells are available in the NCBI GEO (accession numbers GSE124255 and GSE141227, respectively).

Demethylation assay. To measure KDM5 family demethylases activity towards trimethylated H3K4, Flag-KDM5A, Flag-KDM5B, Flag-KDM5C or Flag-KDM5D protein was purified from 293T cells by immunoprecipitation with anti-Flag antibody (F1804, sigma). The histone-demethylase assay was performed as previously described^{38,59}. In brief, the purified Flag-KDM5 proteins were incubated with bulk histones (4 μ g, 10223565001, Sigma) or trimethylated H3K4 peptides (1 μ g, ARTK(me3)QTARKSTGGKAPRKQL, Bankpeptide) in the presence or absence of succinate (Sangon Biotech) in a histone demethylase (HDM) assay buffer (50 mM HEPES pH 8.0, 100 mM [NH₄]₂[SO₄]₂, 1 mM α -KG, 2 mM ascorbate, 5% glycerol and 0.2 mM PMSF) in a final volume of 10 ml for 4–6 h at 37 °C. The reaction mixture was separated by SDS-PAGE, which was followed by western blotting.

Animal studies. All animal studies were conducted with approval from the Animal Research Ethics Committee of University of Science and Technology of China. 5 \times 10⁶ HT1080 cells for each group were injected subcutaneously into 5-week-old male BALB/c nude mice (SJA Laboratory Animal Company). For the in vivo xenograft experiment with dimethyl- α -KG (349631, Sigma) treatment, mice were treated with dimethyl- α -KG (0.6 g per kg (body weight)) or PBS by daily injection, starting day before tumour-cell implantation³⁶. For the xenograft experiment with CPI-455 (T3552, TargetMol) treatment, mice were treated with daily injection of CPI-455 (20 mg per kg (body weight)) or PBS, starting one day before tumour-cell implantation³⁹. Tumours were measured using digital callipers every other day, and tumour volumes were calculated using the following equation: length (mm) \times width (mm) \times depth (mm) \times 0.52. In vivo experiments were randomized to distribute tumour volume among different treatment conditions at the time of treatment initiation.

Clinical human tissue specimen and immunohistochemistry. Formalin-fixed, paraffin-embedded primary DLBCLs and normal lymph-node specimens obtained from 85 patients were randomly selected from the archives of the First Affiliated Hospital of Anhui Medical University. To use these clinical materials for research purposes, written informed consent from patients and approval from the Institutional Research Ethics Committee of the First Affiliated Hospital of Anhui Medical University were obtained. Immunohistochemistry (IHC) was performed as previously described⁶⁰. Images were acquired with a Zeiss AxioImager Z1, and quantification was performed with HistoQuest (TissueGnostics GmbH, Vienna, Austria, www.tissuegnostics.com). The tissue images of ten zones (\times 200 objective) in each sample were analysed to verify the mean optical density (MOD). The MOD data were statistically analysed by the *t* test. The exposure time, signal amplification and objectives were kept the same for all samples when images were obtained. Primary antibodies against the following proteins were used for IHC: Myc (ZA0555, ZSGB-BIO), SDHA (14865-1-AP, Proteintech), SIRT3 (2627, Cell Signaling Technology), new generated antibody against SDHA-K335Ac (Abclonal).

Statistical analysis. The data are presented as the mean \pm s.d. or mean \pm s.e.m. of at least three independent experiments. Student's *t* test was used to calculate *P* values. Statistical significance is displayed as *P* < 0.05.

Reporting Summary. Further information on research design is available in the Nature Research Reporting Summary linked to this article.

Data availability

Data from this study have been deposited in the GEO. Original data from ChIP-seq and RNA-seq in P493 or CA46 cells are available in the NCBI GEO (accession numbers GSE124255 and GSE141227, respectively). The datasets generated and/or analysed during the current study are available from the corresponding author upon reasonable request. Source data for Figs. 1–5 and Extended Data Figs. 1–5 are presented within the paper.

Received: 25 June 2018; Accepted: 11 February 2020;
Published online: 16 March 2020

References

- Eilers, M. & Eisenman, R. N. Myc's broad reach. *Genes Dev.* **22**, 2755–2766 (2008).
- Brooks, T. A. & Hurley, L. H. The role of supercoiling in transcriptional control of MYC and its importance in molecular therapeutics. *Nat. Rev. Cancer* **9**, 849–861 (2009).
- Dang, C. V. MYC on the path to cancer. *Cell* **149**, 22–35 (2012).
- van Riggelen, J., Yetil, A. & Felsher, D. W. MYC as a regulator of ribosome biogenesis and protein synthesis. *Nat. Rev. Cancer* **10**, 301–309 (2010).
- Dang, C. V. MYC, metabolism, cell growth, and tumorigenesis. *Cold Spring Harb. Perspect. Med.* **3**, a014217 (2013).
- Kim, J. W., Gao, P., Liu, Y. C., Semenza, G. L. & Dang, C. V. Hypoxia-inducible factor 1 and dysregulated c-Myc cooperatively induce vascular endothelial growth factor and metabolic switches hexokinase 2 and pyruvate dehydrogenase kinase 1. *Mol. Cell Biol.* **27**, 7381–7393 (2007).
- Zeller, K. I. et al. Global mapping of c-Myc binding sites and target gene networks in human B cells. *Proc. Natl Acad. Sci. USA* **103**, 17834–17839 (2006).
- Guccione, E. et al. Myc-binding-site recognition in the human genome is determined by chromatin context. *Nat. Cell Biol.* **8**, 764–770 (2006).
- Zhang, L., Sokolowski, N., Atmadibrata, B. & Liu, T. Histone demethylase JARID1B promotes cell proliferation but is downregulated by N-Myc oncoprotein. *Oncol. Rep.* **31**, 1935–1939 (2014).
- Ullius, A. et al. The interaction of MYC with the trithorax protein ASH2L promotes gene transcription by regulating H3K27 modification. *Nucleic Acids Res.* **42**, 6901–6920 (2014).
- Santos-Rosa, H. et al. Active genes are tri-methylated at K4 of histone H3. *Nature* **419**, 407–411 (2002).

12. Schneider, R. et al. Histone H3 lysine 4 methylation patterns in higher eukaryotic genes. *Nat. Cell Biol.* **6**, 73–77 (2004).
13. Bernstein, B. E. et al. Genomic maps and comparative analysis of histone modifications in human and mouse. *Cell* **120**, 169–181 (2005).
14. Martinato, F., Cesaroni, M., Amati, B. & Guccione, E. Analysis of Myc-induced histone modifications on target chromatin. *PLoS One* **3**, e3650 (2008).
15. Kim, S. C. et al. Substrate and functional diversity of lysine acetylation revealed by a proteomics survey. *Mol. Cell.* **23**, 607–618 (2006).
16. Choudhary, C. et al. Lysine acetylation targets protein complexes and co-regulates major cellular functions. *Science* **325**, 834–840 (2009).
17. Zhao, S. et al. Regulation of cellular metabolism by protein lysine acetylation. *Science* **327**, 1000–1004 (2010).
18. Wang, Q. et al. Acetylation of metabolic enzymes coordinates carbon source utilization and metabolic flux. *Science* **327**, 1004–1007 (2010).
19. Xiong, Y. & Guan, K. L. Mechanistic insights into the regulation of metabolic enzymes by acetylation. *J. Cell Biol.* **198**, 155–164 (2012).
20. Gil, J., Ramirez-Torres, A. & Encarnacion-Guevara, S. Lysine acetylation and co-regulates a proteomics perspective. *J. Proteomics* **150**, 297–309 (2017).
21. Baysal, B. E. et al. Mutations in SDHD, a mitochondrial complex II gene, in hereditary paraganglioma. *Science* **287**, 848–851 (2000).
22. Hao, H. X. et al. *SDH5*, a gene required for flavination of succinate dehydrogenase, is mutated in paraganglioma. *Science* **325**, 1139–1142 (2009).
23. Hensen, E. F. & Bayley, J. P. Recent advances in the genetics of SDH-related paraganglioma and pheochromocytoma. *Fam. Cancer* **10**, 355–363 (2011).
24. Oermann, E. K., Wu, J., Guan, K. L. & Xiong, Y. Alterations of metabolic genes and metabolites in cancer. *Semin. Cell Dev. Biol.* **23**, 370–380 (2012).
25. Ricketts, C. et al. Germline SDHB mutations and familial renal cell carcinoma. *J. Natl. Cancer Inst.* **100**, 1260–1262 (2008).
26. Kim, S., Kim, D. H., Jung, W. H. & Koo, J. S. Succinate dehydrogenase expression in breast cancer. *Springerplus* **2**, 299 (2013).
27. Cervera, A. M., Bayley, J. P., Devile, P. & McCreath, K. J. Inhibition of succinate dehydrogenase dysregulates histone modification in mammalian cells. *Mol. Cancer* **8**, 89 (2009).
28. Kinnaid, A., Zhao, S., Wellen, K. E. & Michelakis, E. D. Metabolic control of epigenetics in cancer. *Nat. Rev. Cancer* **16**, 694–707 (2016).
29. Letouze, E. et al. SDH mutations establish a hypermethylator phenotype in paraganglioma. *Cancer Cell* **23**, 739–752 (2013).
30. Xiao, M. et al. Inhibition of alpha-KG-dependent histone and DNA demethylases by fumarate and succinate that are accumulated in mutations of FH and SDH tumor suppressors. *Genes Dev.* **26**, 1326–1338 (2012).
31. Lv, L. et al. Acetylation targets the M2 isoform of pyruvate kinase for degradation through chaperone-mediated autophagy and promotes tumor growth. *Mol. Cell* **42**, 719–730 (2011).
32. Zhao, D. et al. Lysine-5 acetylation negatively regulates lactate dehydrogenase A and is decreased in pancreatic cancer. *Cancer Cell* **23**, 464–476 (2013).
33. Tao, R. et al. Sirt3-mediated deacetylation of evolutionarily conserved lysine 122 regulates MnSOD activity in response to stress. *Mol. Cell* **40**, 893–904 (2010).
34. Inuzuka, H. et al. Acetylation-dependent regulation of Skp2 function. *Cell* **150**, 179–193 (2012).
35. Bretones, G. et al. SKP2 oncogene is a direct MYC target gene and MYC down-regulates p27(KIP1) through SKP2 in human leukemia cells. *J. Biol. Chem.* **286**, 9815–9825 (2011).
36. Hoekstra, A. S. et al. Inactivation of SDH and FH cause loss of 5hmC and increased H3K9me3 in paraganglioma/pheochromocytoma and smooth muscle tumors. *Oncotarget* **6**, 38777–38788 (2015).
37. Kooistra, S. M. & Helin, K. Molecular mechanisms and potential functions of histone demethylases. *Nat. Rev. Mol. Cell Biol.* **13**, 297–311 (2012).
38. Liu, P. S. et al. alpha-ketoglutarate orchestrates macrophage activation through metabolic and epigenetic reprogramming. *Nat. Immunol.* **18**, 985–994 (2017).
39. Nie, Z. et al. Structure-based design and discovery of potent and selective KDM5 inhibitors. *Bioorg. Med. Chem. Lett.* **28**, 1490–1494 (2018).
40. Kluk, M. J. et al. Immunohistochemical detection of MYC-driven diffuse large B-cell lymphomas. *PLoS One* **7**, e33813 (2012).
41. Johnson, N. A. et al. Concurrent expression of MYC and BCL2 in diffuse large B-cell lymphoma treated with rituximab plus cyclophosphamide, doxorubicin, vincristine, and prednisone. *J. Clin. Oncol.* **30**, 3452–3459 (2012).
42. Green, T. M. et al. High levels of nuclear MYC protein predict the presence of MYC rearrangement in diffuse large B-cell lymphoma. *Am. J. Surg. Pathol.* **36**, 612–619 (2012).
43. Barrans, S. et al. Rearrangement of MYC is associated with poor prognosis in patients with diffuse large B-cell lymphoma treated in the era of rituximab. *J. Clin. Oncol.* **28**, 3360–3365 (2010).
44. Savage, K. J. et al. MYC gene rearrangements are associated with a poor prognosis in diffuse large B-cell lymphoma patients treated with R-CHOP chemotherapy. *Blood* **114**, 3533–3537 (2009).
45. Carey, C. D. et al. Molecular classification of MYC-driven B-cell lymphomas by targeted gene expression profiling of fixed biopsy specimens. *J. Mol. Diagn.* **17**, 19–30 (2015).
46. Dang, C. V. c-Myc target genes involved in cell growth, apoptosis, and metabolism. *Mol. Cell Biol.* **19**, 1–11 (1999).
47. Zhao, D. et al. NOTCH-induced aldehyde dehydrogenase 1A1 deacetylation promotes breast cancer stem cells. *J. Clin. Invest.* **124**, 5453–5465 (2014).
48. Yang, H. et al. SIRT3-dependent GOT2 acetylation status affects the malate-aspartate NADH shuttle activity and pancreatic tumor growth. *EMBO J.* **34**, 1110–1125 (2015).
49. Fan, J. et al. Tyr phosphorylation of PDP1 toggles recruitment between ACAT1 and SIRT3 to regulate the pyruvate dehydrogenase complex. *Mol. Cell* **53**, 534–548 (2014).
50. Zhang, M. et al. Sirtinol promotes PEPCK1 degradation and inhibits gluconeogenesis by inhibiting deacetylase SIRT2. *Sci. Rep.* **7**, 7 (2017).
51. Gao, P. et al. c-Myc suppression of miR-23a/b enhances mitochondrial glutaminase expression and glutamine metabolism. *Nature* **458**, 762–765 (2009).
52. Sun, L. et al. cMyc-mediated activation of serine biosynthesis pathway is critical for cancer progression under nutrient deprivation conditions. *Cell Res.* **25**, 429–444 (2015).
53. Wu, G. et al. Menin enhances c-Myc-mediated transcription to promote cancer progression. *Nat. Commun.* **8**, 15278 (2017).
54. Miettinen, M. et al. Succinate dehydrogenase-deficient GISTs: a clinicopathologic, immunohistochemical, and molecular genetic study of 66 gastric GISTs with predilection to young age. *Am. J. Surg. Pathol.* **35**, 1712–1721 (2011).
55. Badve, S. et al. Basal-like and triple-negative breast cancers: a critical review with an emphasis on the implications for pathologists and oncologists. *Mod. Pathol.* **24**, 157–167 (2011).
56. Schuhmacher, M. et al. Control of cell growth by c-Myc in the absence of cell division. *Curr. Biol.* **9**, 1255–1258 (1999).
57. Guan, K. L., Yu, W., Lin, Y., Xiong, Y. & Zhao, S. Generation of acetyllysine antibodies and affinity enrichment of acetylated peptides. *Nat. Protoc.* **5**, 1583–1595 (2010).
58. Lee, M. G., Wynder, C., Norman, J. & Shiekhhattar, R. Isolation and characterization of histone H3 lysine 4 demethylase-containing complexes. *Methods* **40**, 327–330 (2006).
59. Xu, W. et al. Oncometabolite 2-hydroxyglutarate is a competitive inhibitor of alpha-ketoglutarate-dependent dioxygenases. *Cancer Cell* **19**, 17–30 (2011).
60. Lei, Q. et al. NKX3.1 stabilizes p53, inhibits AKT activation, and blocks prostate cancer initiation caused by PTEN loss. *Cancer Cell.* **9**, 367–378 (2006).

Acknowledgements

We thank C. V. Dang for critical reading of this manuscript and valuable suggestions. This work is supported in part by National Natural Science Foundation of China (91957203, 81525022, 81930083, 31571472, 81530076, 81821001), National Key R&D Program of China (2018YFA0800300, 2018YFA0107103, 2017YFA0205600), the Chinese Academy of Sciences (XDPB10), the Program for Guangdong Introducing Innovative and Entrepreneurial Teams (2017ZT07S054) and the Program of Development Foundation of Hefei Center for Physical Science and Technology (2017FXZY004). Please address all the correspondence and requests for materials to P.G. (pgao2@ustc.edu.cn).

Author contributions

P.G. and H.Z. conceived the study and supervised the experiments. S.-T.L., D.H., P.G., X.D. and H.Z. designed the experiments. X.D. performed and analysed MS mitochondrial protein acetylation. S.-T.L., D.H., S.X., G.W., Z.J., Y.H., M.Y., N.W., R.Y., D.Y., L.W., Z.L. and X.H. performed experiments. S.S., L.Z. and K.Q. analysed ChIP-seq data and RNA-seq data. Y.C. provided clinical specimens. R.Z. and A.L. provided constructive guidance and advice. P.G., H.Z., D.H. and S.-T.L. wrote the paper. All the authors read and approved the manuscript.

Competing interests

The authors declare no competing interests.

Additional information

Extended data is available for this paper at <https://doi.org/10.1038/s42255-020-0179-8>.

Supplementary information is available for this paper at <https://doi.org/10.1038/s42255-020-0179-8>.

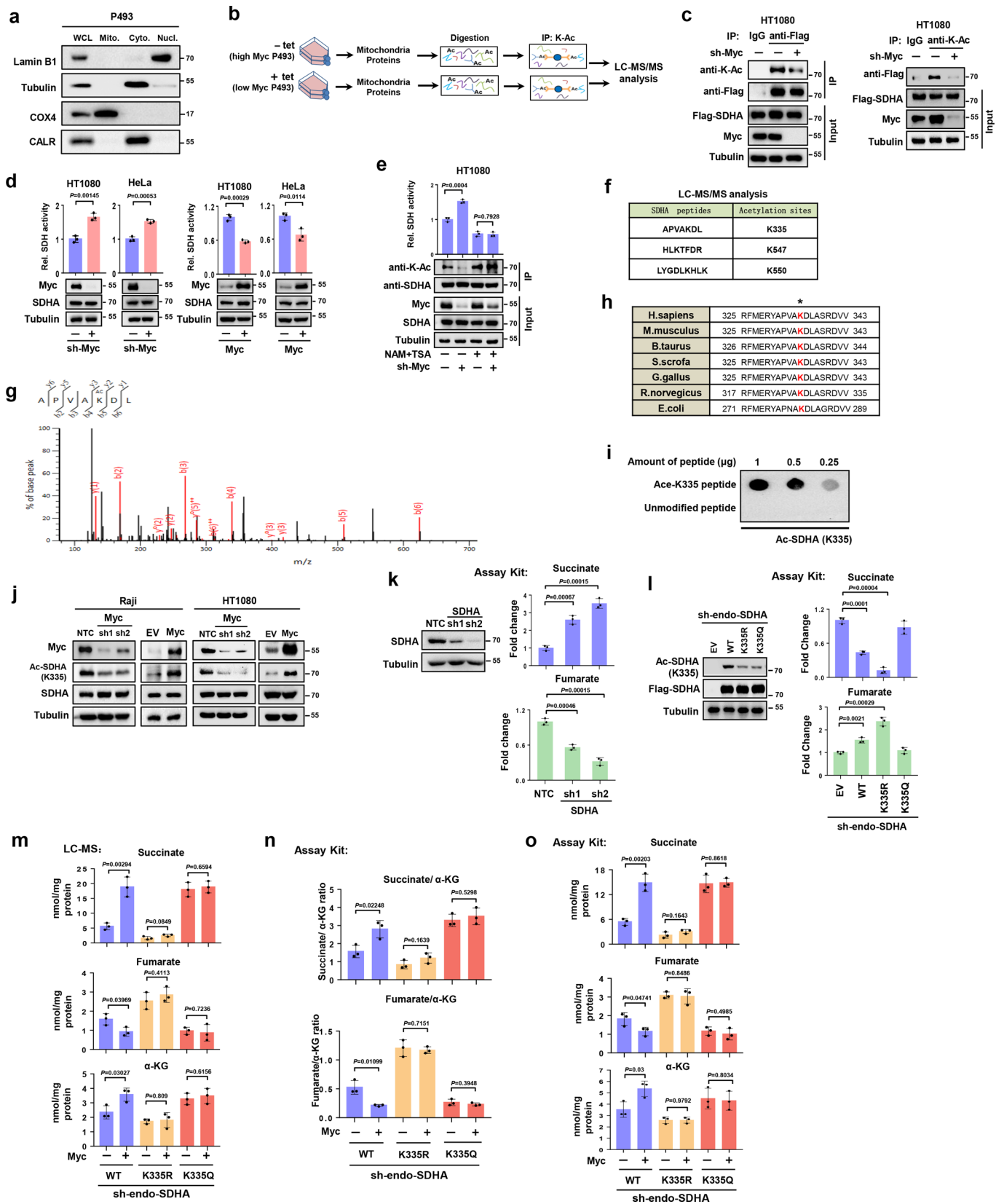
Correspondence and requests for materials should be addressed to X.D., H.Z. or P.G.

Peer review information Primary Handling Editors: Ana Mateus; Elena Bellafante.

Reprints and permissions information is available at www.nature.com/reprints.

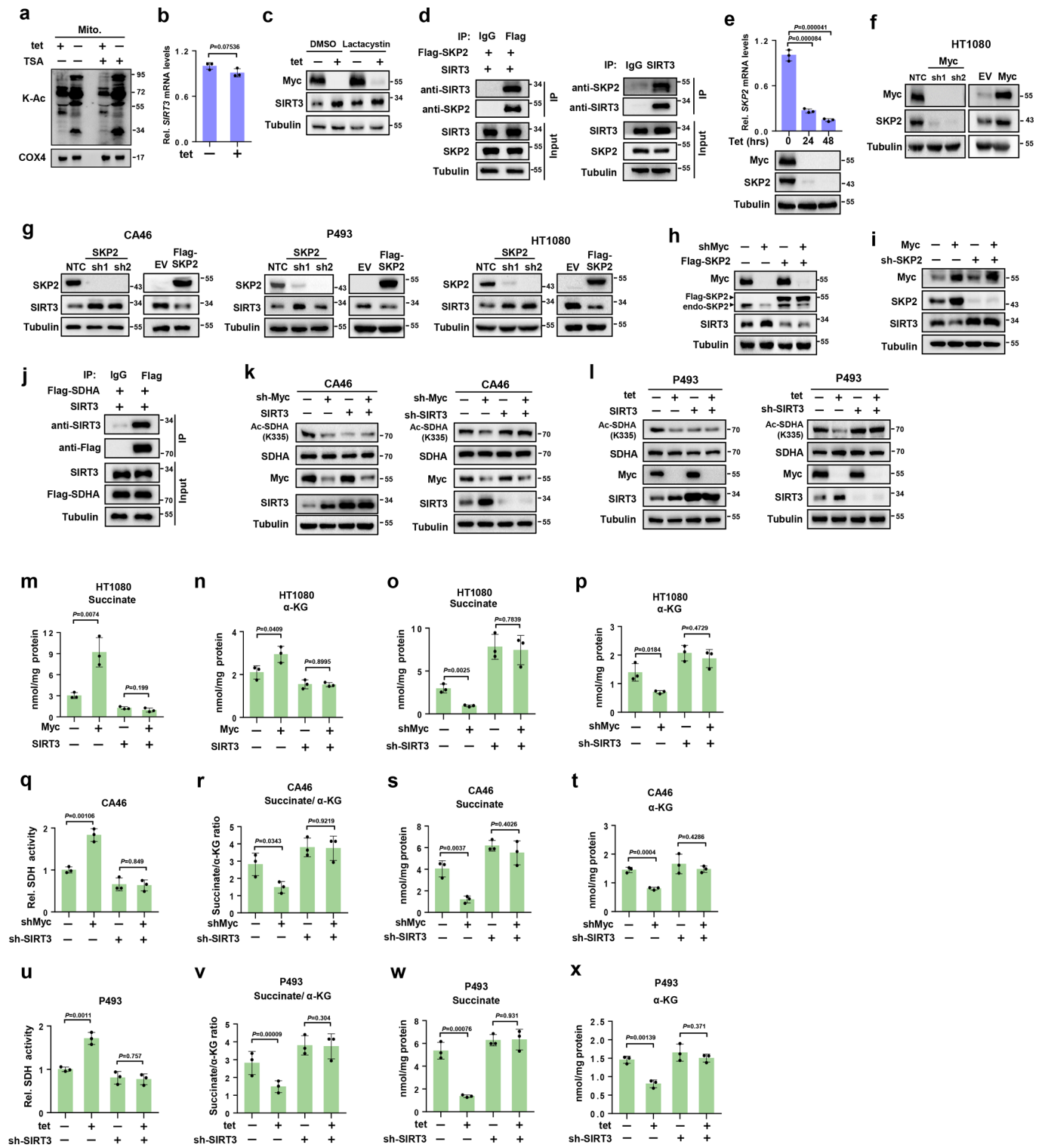
Publisher's note Springer Nature remains neutral with regard to jurisdictional claims in published maps and institutional affiliations.

© The Author(s), under exclusive license to Springer Nature Limited 2020



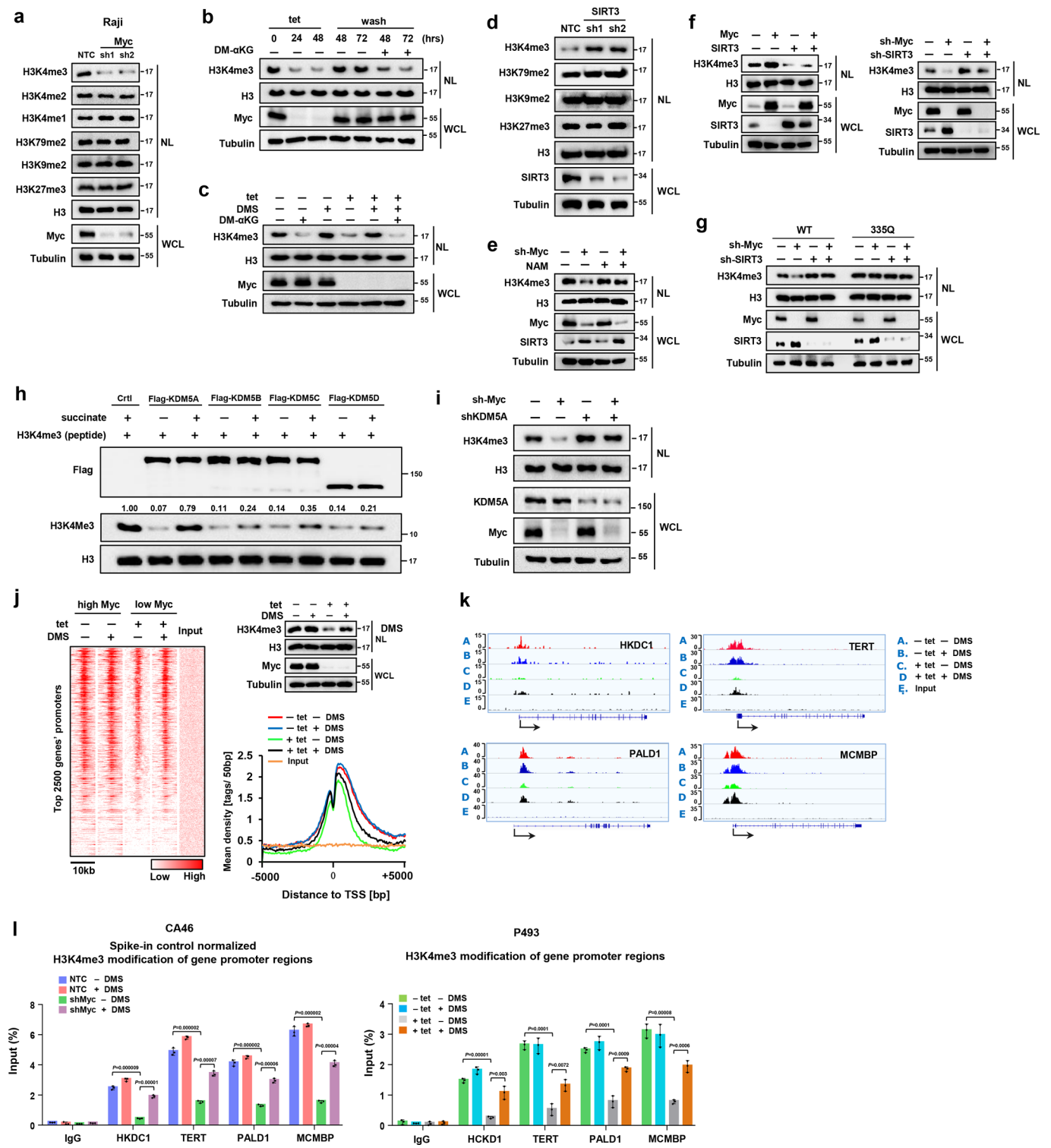
Extended Data Fig. 1 | See next page for caption.

Extended Data Fig. 1 | Myc inhibits SDH complex activity and causes cellular succinate accumulation by inducing SDHA acetylation. **a**, Western blot analysis of the nuclear marker lamin B1, cytoplasmic marker tubulin, endoplasmic reticulum marker CALR (Calreticulin) and mitochondrial marker COX4 (cytochrome c oxidase subunit IV) using the whole cell lysates or purified subcellular fractions from P493 cells. **b**, Diagram showing extraction of the mitochondrial fraction after P493 cells were treated with or without tetracycline (tet) for 48 hours. Mitochondrial proteins were digested, and lysine-acetylated peptides were immunoprecipitated using acetylated-lysine antibody. Enriched acetylated peptides were analyzed by nano LC-MS/MS (see Materials and Methods). **c**, HT1080 cells stably expressing flag-SDHA were further infected with viruses expressing non-targeting control (NTC) or Myc shRNA, followed by immunoprecipitation using anti-flag antibody, IgG (*left panel*) or using anti-lysine-acetylation antibody (anti-K-Ac) or IgG (*right panel*). Western blot analysis of Myc, flag-SDHA and SDHA acetylation. **d**, SDH activity was measured in HT1080 and HeLa cells infected with viruses expressing NTC or Myc shRNA for 48 hours (*left panel*), or in HT1080 and HeLa cells infected with pMX-GFP empty vector (EV) or pMX-GFP-Myc vector (*right panel*). Myc and SDHA expression were analyzed by western blotting. Data are presented as the mean \pm SD of three independent experiments ($n=3$). Group differences are analyzed by the two-tailed Student's t-test. $P < 0.05$ compared with the NTC or EV group. **e**, SDH activity was measured in HT1080 cells infected with viruses expressing NTC or Myc shRNA (*right panel*) and further exposed to 10 mM NAM and 1 μ M TSA. Immunoprecipitation assay using anti-SDHA antibody was performed using the above conditions. SDH activity was normalized to protein content. Data are presented as the mean \pm SD of three independent experiments ($n=3$). Group differences are analyzed by the two-tailed Student's t-test. $P < 0.05$ compared with the corresponding control group. **f**, K335, K547 and K550 acetylated sites of SDHA were determined by LC-MS/MS. **g**, LC-MS/MS spectrum of the K335 acetylated peptide of SDHA. **h**, Primary sequence alignment of acetylated peptides from the indicated species. * denotes the acetylated K335 residues detected by nano LC-MS/MS. **i**, Validation of the acetyl-SDHA (K335) antibody by dot blot using a nitrocellulose membrane spotted with acetylated K335 peptide or unmodified peptide at the indicated concentration. **j**, Western blot analysis of Myc, SDHA K335 acetylation and endogenous SDHA levels in Raji cells expressing NTC or Myc shRNAs (sh1 and sh2), or in HT1080 cells expressing pMX-GFP empty vector (EV) or pMX-GFP-Myc vector. **k**, Western blot analysis of SDHA expression in HT1080 cells infected with viruses expressing NTC or SDHA shRNAs (sh1 and sh2). Cellular succinate and fumarate levels were determined using assay kits. Data are presented as the mean \pm SD of three independent experiments ($n=3$). Group differences are analyzed by the two-tailed Student's t-test. $P < 0.05$ compared with the NTC group. **l**, HT1080 cells with stable knockdown of endogenous SDHA were subsequently infected with viruses expressing flag-wild-type-SDHA (WT), flag-SDHA^{K335R} (K335R) or flag-SDHA^{K335Q} (K335Q), followed by western blot analysis of SDHA K335 acetylation and measurement of succinate and fumarate. Relative succinate or fumarate levels of triplicate experiments mean \pm SD are presented ($n=3$). Group differences are analyzed by the two-tailed Student's t-test. $P < 0.05$ compared with the EV group. **m**, Cellular succinate, fumarate or α -KG levels were determined using the LC-MS in the HT1080 cells used in (Fig. 1i, *right panel*). The metabolic measurements of LC-MS were normalized to cellular protein. Metabolites level of triplicate experiments mean \pm SD are presented ($n=3$). Group differences are analyzed by the two-tailed Student's t-test. $P < 0.05$ compared with the indicated group. **n** and **o**, Cellular succinate, fumarate or α -KG levels were determined by assay kits in the HT1080 cells used in (Fig. 1i, *right panel*) (**o**), then succinate/ α -KG ratio or fumarate/ α -KG ratio was calculated (**n**). The metabolic measurements of LC-MS were normalized to cellular protein. Data are presented as the mean \pm SD of three independent experiments ($n=3$). Group differences are analyzed by the two-tailed Student's t-test. $P < 0.05$ compared with the indicated group. $n=3$ independent experiments were repeated with similar results (**a**, **c**, **i**, and **j**). Two independent LC-MS/MS experiments in P493 cells were repeated with similar results (**g**).



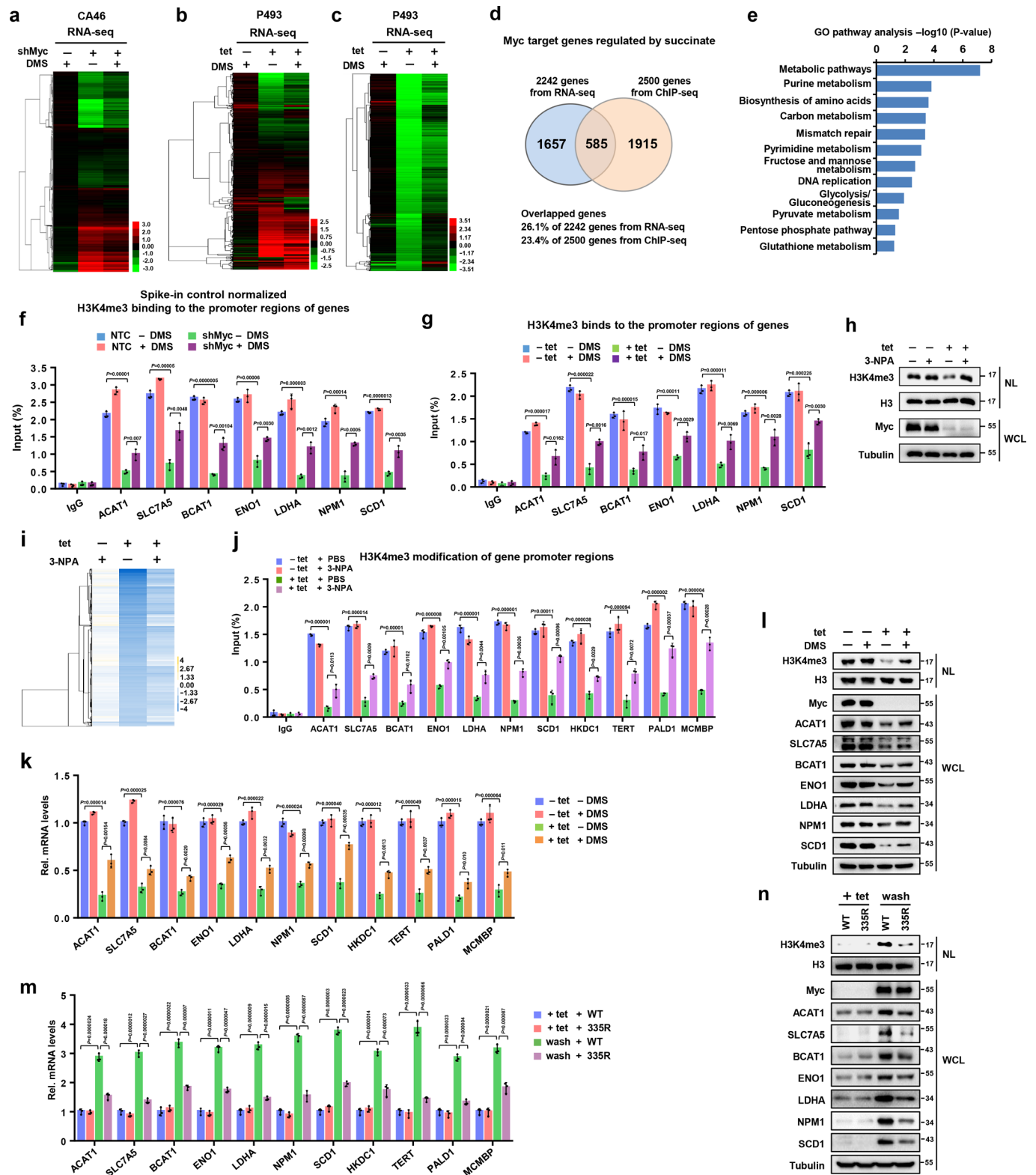
Extended Data Fig. 2 | See next page for caption.

Extended Data Fig. 2 | Myc increases SDHA acetylation by accelerating SKP2-mediated proteasomal degradation of SIRT3. **a**, Mitochondrial proteins from P493 cells treated with or without tetracycline (tet) for 48 hours were cultured in the presence of vehicle or 1 μ M TSA for 18 hours, followed by western blot analysis of lysine-acetylation (K-Ac). COX4 served as a loading control. **b**, Quantitative real-time PCR analysis of SIRT3 mRNA levels in P493 cells treated with or without tetracycline (tet) for 24 hours. Data are presented as the mean \pm SD of three independent experiments ($n=3$). Group differences are analyzed by the two-tailed Student's t-test. $P < 0.05$ compared with the indicated group. **c**, Western blot analysis of SIRT3 in P493 cells treated with or without tetracycline (tet) for 48 hours and further cultured in the presence of vehicle or 10 μ M lactacystin for 8 hours. Tubulin served as a loading control. **d**, Immunoprecipitation was performed using anti-flag antibody or IgG in HEK293T cells transfected with flag-SKP2 and SIRT3, followed by western blot analysis of SIRT3 and SKP2 (*left panel*). Immunoprecipitation was performed using anti-SIRT3 antibody or IgG in HT1080 cells, followed by western blot of SIRT3 and SKP2 (*right panel*). Tubulin served as a loading control. **e**, Quantitative real-time PCR and western blot analysis of SKP2 expression in P493 cells treated with or without tetracycline (tet) for 24 and 48 hours. Data are presented as the mean \pm SD of three independent experiments ($n=3$). Group differences are analyzed by the two-tailed Student's t-test. $P < 0.05$ compared with the indicated group. **f**, Western blot analysis of SKP2 in HT1080 cells infected with viruses expressing NTC or Myc shRNA (*left panel*) or in HT1080 cells infected with viruses expressing pMX-GFP empty vector (EV) or pMX-GFP-Myc vector (*right panel*). Tubulin served as a loading control. **g**, Western blot analysis of SKP2 and SIRT3 protein in P493 cells (*upper left panel*), HT1080 cells (*bottom left panel*) or CA46 cells (*right panel*) infected with viruses expressing NTC or SKP2 shRNAs (sh1 and sh2), or infected with EV or pSIN-3xflag-SKP2. Tubulin served as a loading control. **h**, HT1080 cells stably expressing NTC or Myc shRNA were subsequently infected with viruses expressing empty vector (EV) or flag-SKP2 vector, followed by western blot analysis of Myc, flag-SKP2 and SIRT3 expression. **i**, HT1080 cells stably expressing NTC or SKP2 shRNAs were subsequently infected with viruses of EV or Myc, followed by western blot analysis of Myc, SKP2 and SIRT3 expression. Tubulin served as a loading control. **j**, Immunoprecipitation was performed using anti-flag antibody or IgG in HEK293T cells transfected with flag-SDHA and SIRT3, followed by western blot analysis of SIRT3 and flag-SDHA. **k**, CA46 cells stably expressing empty vector (EV) or SIRT3 were subsequently infected with viruses expressing NTC or Myc shRNA (*left panel*), or CA46 cells stably expressing NTC or SIRT3 shRNA were further infected with viruses expressing NTC or Myc shRNA (*right panel*), followed by western blot analysis of Myc, SIRT3, SDHA and SDHA K335 acetylation. **l**, P493 cells stably expressing EV or 3xflag-SIRT3 were treated with or without tetracycline (tet) for 48 hours, (*left panel*). P493 cells stably expressing NTC or SIRT3 shRNA were treated with or without tetracycline (tet) for 48 hours (*right panel*), followed by western blot analysis of SDHA K335 acetylation, SDHA, SIRT3 and Myc. Tubulin served as a loading control. **m-p**, Cellular succinate or α -KG levels were determined by LC-MS in the HT1080 cells used in Fig. 2i, then succinate/ α -KG ratio was calculated. The succinate or α -KG levels were normalized to cellular protein. Succinate or α -KG level of triplicate experiments mean \pm SD are presented ($n=3$). Group differences are analyzed by the two-tailed Student's t-test. $P < 0.05$ compared with the indicated group. **q**, Measurement of SDH activity in the CA46 cells used in (**k**, *right panel*). Relative enzyme activities of triplicate experiments mean \pm SD are presented ($n=3$). Group differences are analyzed by the two-tailed Student's t-test. $P < 0.05$ compared with the indicated group. **r-t**, Cellular succinate or α -KG levels were determined with LC-MS in the CA46 cells used in (**k**, *right panel*), then succinate/ α -KG ratio was calculated (**r**). The succinate or α -KG levels were normalized to cellular protein (**s**, **t**). Succinate or α -KG level of triplicate experiments mean \pm SD are presented ($n=3$). Group differences are analyzed by the two-tailed Student's t-test. $P < 0.05$ compared with the indicated group. **u**, Measurement of SDH activity in the P493 cells used in (**l**, *right panel*). Relative enzyme activities of triplicate experiments \pm SD are presented ($n=3$). Group differences are analyzed by the two-tailed Student's t-test. $P < 0.05$ compared with the indicated group. **v-x**, Cellular succinate or α -KG levels were determined with LC-MS in the P493 cells used in (**l**, *right panel*), then succinate/ α -KG ratio was calculated (**v**). The succinate or α -KG levels were normalized to cellular protein (**w**, **x**). Succinate or α -KG level of triplicate experiments mean \pm SD are presented ($n=3$). Group differences are analyzed by the two-tailed Student's t-test. $P < 0.05$ compared with the indicated group. $n=3$ independent experiments were repeated with similar results (**a**, **c**, **d** and **f-l**).



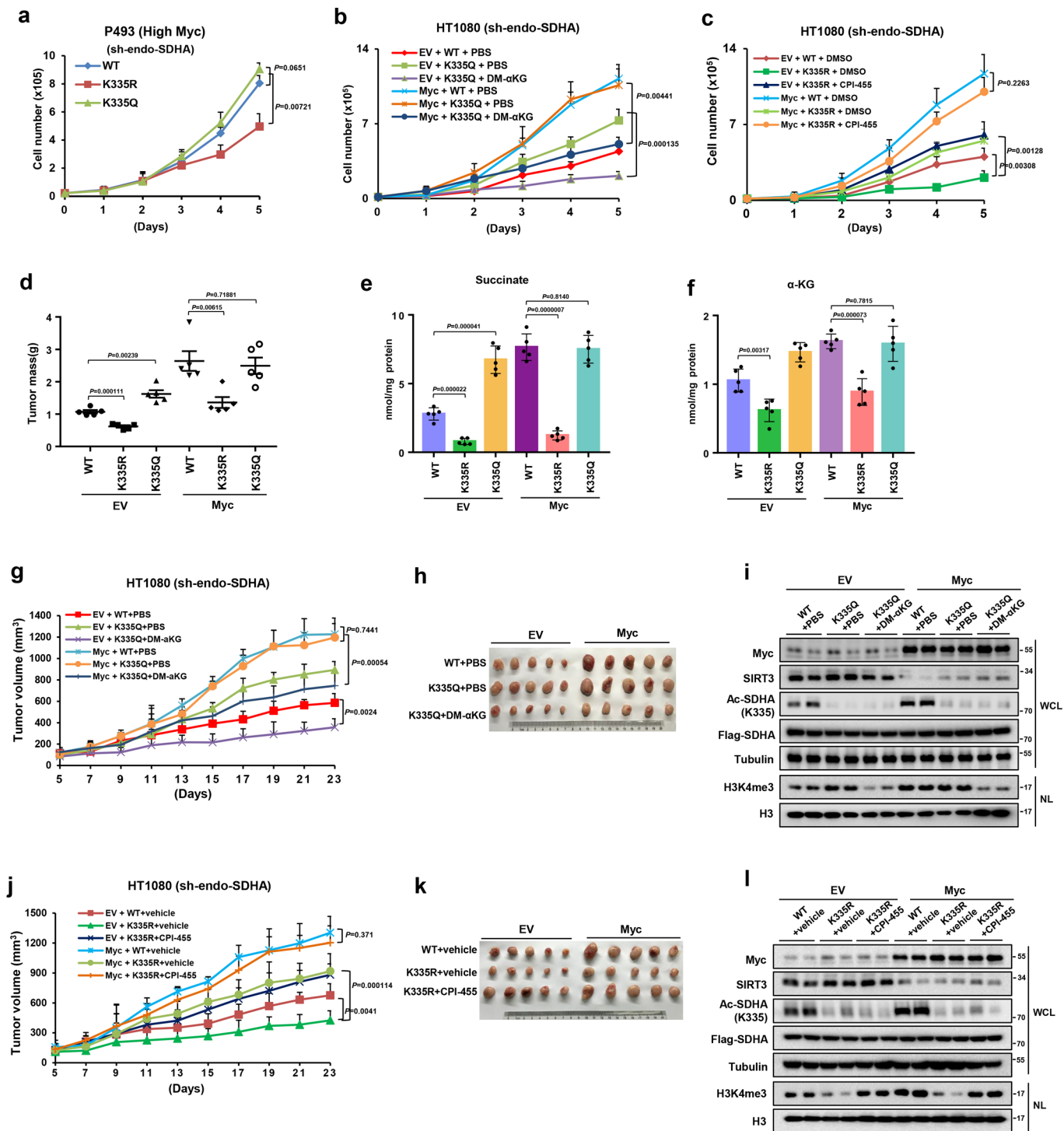
Extended Data Fig. 3 | See next page for caption.

Extended Data Fig. 3 | Myc enhances H3K4me3 via SDHA acetylation-mediated increase in cellular succinate. **a**, Western blot analysis of the indicated histone methylation markers and Myc in Raji cells infected with viruses expressing NTC or Myc shRNAs (sh1, sh2). **b**, P493 cells treated with or without tetracycline (tet) were exposed to 5 mM dimethyl α -KG (DM- α KG) for 8 hours, followed by western blot analysis of H3K4me3 and Myc from nuclear lysates and whole cell lysates, respectively. **c**, P493 cells treated with or without tetracycline (tet) were exposed to 10 mM dimethyl succinate (DMS) or/ and 5 mM dimethyl α -KG (DM- α KG), followed by western blot analysis of H3K4me3 and Myc from nuclear lysates and whole cell lysates, respectively. H3 and tubulin served as loading controls. **d**, Western blot analysis of the indicated histone methylation markers from nuclear lysates and whole cell lysates in HT1080 cells infected with viruses expressing NTC or SIRT3 shRNAs (sh1 and sh2). Tubulin and H3 served as loading controls. WCL, whole-cell lysate; NL, nuclear lysate. **e**, HT1080 cells infected with viruses of NTC or Myc shRNA were cultured in the presence of vehicle or 10 mM NAM, followed by western blot analysis of H3K4me3, Myc and SIRT3 from nuclear lysates and whole cell lysates. Tubulin and H3 served as loading controls. WCL, whole-cell lysates; NL, nuclear lysates. **f**, HT1080 cells stably expressing pSIN-EV empty vector (EV) or pSIN-SIRT3 vector were subsequently infected with viruses expressing pMX-GFP empty vector (EV) or pMX-GFP-Myc vector (*left panel*), or HT1080 cells stably expressing NTC or SIRT3 shRNA were subsequently infected with viruses expressing NTC or Myc shRNA (*right panel*), followed by western blot analysis of H3K4me3, Myc and SIRT3 levels. **g**, HT1080 cells with stable knockdown of endogenous SDHA were infected with viruses expressing flag-wild-type-SDHA (WT) or flag-SDHA^{K335Q} (K335Q), followed by further infection with viruses of NTC or SIRT3 shRNA and NTC or Myc shRNA. Western blot analysis of H3K4me3, Myc and SIRT3 levels. **h**, Western blot analysis of the *in vitro* demethylation reactions using H3K4me3 peptide as substrates. Antibodies used are indicated. **i**, HT1080 cells stably expressing NTC or sh-Myc were subsequently infected with viruses expressing NTC or sh-KDM5A, followed by western blot analysis of Myc, H3K4me3, KDM5A, H3 and tubulin expression. WCL, whole-cell lysates; NL, nuclear lysates. **j**, P493 cells treated with or without tetracycline (tet) for 48 h were cultured in the presence of vehicle or 10 mM dimethyl succinate (DMS) for 24 h, followed by western blot analysis of H3K4me3 (*up right panel*) and ChIP-seq analysis of H3K4me3 around gene TSS regions. Heat map showing H3K4me3 levels in TSS regions for the top 2500 gene promoters (*left panel*). Distribution analysis of H3K4me3 tags around the TSS regions of the top 2500 genes (*bottom right panel*). $n=3$ independent experiments for western blot (*up right panel*) were repeated with similar results. One replicate ($n=1$, each group) was used for ChIP-seq assay of P493 cells. **k**, H3K4me3 markers of ChIP-sequencing traces in P493 cells for the indicated genes were determined by IGV software analysis. For IGV analysis, one replicate ($n=1$, each group) was used for H3K4me3 analysis in ChIP-seq assay of P493 cells. **l**, ChIP assay analysis of the occupancy of H3K4me3 on the indicated gene promoters in the CA46 cells used in Fig. 3g (*left panel*) or P493 cells used in Extended Data Fig. 3j (*right panel*). Data are presented as the mean \pm SD of three independent experiments ($n=3$). Group differences are analyzed by the two-tailed Student's *t*-test. $P < 0.05$ compared with the NTC-DMS group or shMyc-DMS group (*left panel*); $P < 0.05$ compared with the -tet-DMS group or +tet-DMS group (*right panel*). $n=3$ independent experiments were repeated with similar results (**a-i**).



Extended Data Fig. 4 | See next page for caption.

Extended Data Fig. 4 | Myc-mediated succinate accumulation and H3K4me3 activation promote its target gene expression. **a**, CA46 cells treated with viruses expressing NTC or Myc shRNAs were cultured in the presence of vehicle or 10 mM dimethyl-succinate (DMS) for 24 hours, followed by the extraction of total RNAs for the RNA-Seq experiment. Heat map showing all the regulated genes. **b**, P493 cells treated with or without tetracycline (tet) were cultured in the presence of vehicle or 10 mM dimethyl-succinate (DMS) for 24 hours, followed by the extraction of total RNAs for the RNA-Seq experiment. Heat map showing all the regulated genes. **c**, Heat map of the RNA-seq results showing that the genes with down-regulated expression following Myc depletion were subsequently rescued by DMS treatment in P493 cells (fold-change >1.5). **d**, Venn diagram showing overlapping genes co-regulated by Myc and succinate based on the RNA-Seq data and ChIP-Seq data in P493 cells. Correlation significance between genes with mRNA levels and genes with H3K4me3 that were rescued by DMS based on RNA-seq and ChIP-seq, respectively, were determined using a two-tailed Spearman test, $P < 0.001$. **e**, Analysis of 585 overlapping genes by Gene Ontology (GO) term enrichment. P values were analysed with two-tailed Student's t -test. The sufficient RNA-seq samples ($n = 1$, each group) were analyzed in Gene Ontology (GO) term enrichment. **f**, ChIP assay analysis of the occupancy of H3K4me3 on the indicated gene promoters in the CA46 cells used in **(a)**. Data are presented as the mean \pm SD of three independent experiments ($n = 3$). Group differences are analyzed by the two-tailed Student's t -test. $P < 0.05$ compared with the NTC -DMS group; $P < 0.05$ compared with the shMyc-DMS group. **g**, ChIP assay analysis of the occupancy of H3K4me3 on the indicated gene promoters in the P493 cells used in **(b)**. Data are presented as the mean \pm SD of three independent experiments. Group differences are analyzed by the two-tailed Student's t -test. $P < 0.05$ compared with the -tet -DMS group; $P < 0.05$ compared with the +tet -DMS group. **h**, P493 cells treated with or without tetracycline (tet) for 48 hours were cultured in the presence of vehicle or 500 μ M 3-nitropropionic acid (3-NPA) for 24 hours, followed by western blot analysis of H3K4me3. **i**, Heat map of the RNA-seq data showing that the genes with down-regulated expression following Myc depletion were markedly rescued by 3-NPA treatment in P493 cells (fold-change >1.5). The statistical significance between Myc- and succinate-regulated genes was determined using Fisher's exact probability, $P < 0.001$. The RNA-seq samples ($n = 1$, each group) used to analysed for Heatmap. **j**, ChIP assay studying the occupancy of H3K4me3 on the indicated gene promoters in the P493 cells used in **(i)**. Data are presented as the mean \pm SD of three independent experiments ($n = 3$). Group differences are analyzed by the two-tailed Student's t -test. $P < 0.05$ compared to the -tet +PBS group; $P < 0.05$ compared to the +tet +PBS group. **k**, The mRNA levels of the indicated genes were determined by RT-qPCR in the P493 cells used in **(b)**. Data are presented as the mean \pm SD of three independent experiments ($n = 3$). Group differences are analyzed by the two-tailed Student's t -test. $P < 0.05$ compared with the -tet -DMS group; $P < 0.05$ compared with the +tet -DMS group. **l**, The indicated proteins were determined by western blotting in the P493 cells used in **(k)**. **m**, P493 cells with endogenous SDHA knockdown were further constructed to stably express flag-wild-type-SDHA (WT) or flag-SDHA^{K335R} (K335R), followed by treatment with tetracycline (tet) for 48 h or washing to remove tet for 48 hours. The mRNA levels of the indicated genes were determined by RT-qPCR. Data are presented as the mean \pm SD of three independent experiments ($n = 3$). Group differences are analyzed by the two-tailed Student's t -test. $P < 0.05$ compared with the +tet +WT group; $P < 0.05$ compared with the wash +WT group. **n**, The indicated proteins were determined by western blotting in the P493 cells used in **(m)**. The statistical significance between Myc- and succinate-regulated genes was determined using the two-sided Fisher's exact probability, $P < 0.001$. The sufficient RNA-seq samples ($n = 1$, each group) used to analysed for Heatmap **(a-c)**. $n = 3$ independent experiments were repeated with similar results **(h, l and n)**. Tubulin and H3 served as loading controls. WCL, whole-cell lysates; NL, nuclear lysates.



Extended Data Fig. 5 | See next page for caption.

Extended Data Fig. 5 | SDHA acetylation at lysine 335 contributes to Myc-promoted tumour progression. **a**, P493 cells with stable knockdown of endogenous SDHA were further infected with viruses expressing flag-wild-type-SDHA (WT), flag-SDHA^{K335R} (K335R) or flag-SDHA^{K335Q} (K335Q). Cell growth curves were determined by trypan blue counting. Data are presented as the mean \pm SD ($n=3$, each group). Group differences are analyzed by the two-tailed Student's *t*-test. $P < 0.05$ compared with the corresponding indicated group. **b**, Endogenous SDHA was knocked down in empty vector (EV) or Myc overexpressing HT1080 cells, followed by further infection with viruses expressing flag-wild-type-SDHA (WT) or flag-SDHA-K335Q (K335Q). The cells were treated with or without 5 mM dimethyl α -KG (DM- α KG) (fresh medium containing fresh DM- α KG was replaced daily), and the cell growth of HT1080 cells was determined by trypan blue staining. Data are presented as the mean \pm SD ($n=5$, each group). Group differences are analyzed by the two-tailed Student's *t*-test. $P < 0.05$ compared between indicated groups. **c**, Endogenous SDHA was knocked down in empty vector (EV) or Myc overexpressing HT1080 cells, followed by further infection with viruses expressing flag-wild-type-SDHA (WT) or flag-SDHA-K335R (K335R). The cells were treated with or without 5 μ M CPI-455, followed by cell growth analysis with trypan blue staining. Data are presented as the mean \pm SD ($n=3$, each group). Group differences are analyzed by the two-tailed Student's *t*-test. $P < 0.05$ compared with the indicated group. **d**, The tumor mass of the extracted tumors in Fig. 5d was measured. Data are presented as mean \pm SEM ($n=5$, each group). Group differences are analyzed by the two-tailed Student's *t*-test. $P < 0.05$ compared with the corresponding indicated group. **e** and **f**, The succinate and α -KG levels were measured using detection kits with cell lysates from xenograft tumor tissues. The succinate and α -KG level were normalized to cellular protein. Data are presented as the mean \pm SD ($n=5$, each group). Group differences are analyzed by the two-tailed Student's *t*-test. $P < 0.05$ compared with the indicated group. **g** and **h**, HT1080 cells used in **b** were injected subcutaneously into BALB/c nude mice ($n=5$, each group). Mice were treated with daily i.p injection of Dimethyl α -KG (0.6 g/kg body weight) or PBS, starting one day before tumor cell implantation. Tumor growth curves were measured starting from 5 days after inoculation (**g**). Tumors were extracted and compared at the end of the experiment (**h**). Data are presented as the mean \pm SD ($n=5$, each group). Group differences are analyzed by the two-tailed Student's *t*-test. $P < 0.05$ compared between indicated groups. **i**, Levels of Myc, SIRT3, SDHA, and K335 acetylation of SDHA and H3K4me3 were determined by western blot using the nuclear lysates or whole cell lysates of tumor tissues from each group as in **h**. $n=5$ independent xenograft tumor tissues lysates in each group were repeated by western blot with similar results. Tubulin and H3 served as loading controls. WCL, whole cell lysates; NL, nuclear lysates. **j** and **k**, HT1080 cells used in **c** were injected subcutaneously into BALB/c nude mice ($n=5$ for each group). Mice were treated with daily i.p injection of CPI-455 (20 mg/kg body weight) or vehicle (4%DMSO + 35%PEG 300 + 2%Tween 80+PBS), starting one day before tumor cell implantation. Tumor growth curves were measured starting from 5 days after inoculation (**j**). Tumors were extracted and compared at the end of the experiment (**k**). Data are presented as the mean \pm SD ($n=5$, each group). Group differences are analyzed by the two-tailed Student's *t*-test. $P < 0.05$ compared between indicated groups. **l**, Levels of Myc, SIRT3, SDHA, and K335 acetylation of SDHA and H3K4me3 were determined by western blot using the nuclear lysates or whole cell lysates of tumor tissues from each group as in **k**. Tubulin and H3 served as loading controls. WCL, whole-cell lysates; NL, nuclear lysates. $n=5$ independent xenograft tumor tissues lysates in each group were repeated by western blot with similar results.

Reporting Summary

Nature Research wishes to improve the reproducibility of the work that we publish. This form provides structure for consistency and transparency in reporting. For further information on Nature Research policies, see [Authors & Referees](#) and the [Editorial Policy Checklist](#).

Statistics

For all statistical analyses, confirm that the following items are present in the figure legend, table legend, main text, or Methods section.

n/a Confirmed

- The exact sample size (n) for each experimental group/condition, given as a discrete number and unit of measurement
- A statement on whether measurements were taken from distinct samples or whether the same sample was measured repeatedly
- The statistical test(s) used AND whether they are one- or two-sided
Only common tests should be described solely by name; describe more complex techniques in the Methods section.
- A description of all covariates tested
- A description of any assumptions or corrections, such as tests of normality and adjustment for multiple comparisons
- A full description of the statistical parameters including central tendency (e.g. means) or other basic estimates (e.g. regression coefficient) AND variation (e.g. standard deviation) or associated estimates of uncertainty (e.g. confidence intervals)
- For null hypothesis testing, the test statistic (e.g. F , t , r) with confidence intervals, effect sizes, degrees of freedom and P value noted
Give P values as exact values whenever suitable.
- For Bayesian analysis, information on the choice of priors and Markov chain Monte Carlo settings
- For hierarchical and complex designs, identification of the appropriate level for tests and full reporting of outcomes
- Estimates of effect sizes (e.g. Cohen's d , Pearson's r), indicating how they were calculated

Our web collection on [statistics for biologists](#) contains articles on many of the points above.

Software and code

Policy information about [availability of computer code](#)

Data collection

Q-Exactive mass spectrometer (Thermo Fisher, SJ) was used to collect mitochondrial protein acetylation data. Sciex Analyst 1.7.1 instrument acquiring software (AB SCIEX) were used to collect and analyze metabolites of LC-MS data; Illumina Hiseq4000 platform (Novogene, Tianjing, China) was used to collect RNA-seq data; Illumina Hiseq2500 platform (BGI, Shenzhen, China) was used to collect ChIP-seq data for P493 cells; Illumina novaseq6000 platform (Novogene, Tianjin, China) was used to collect ChIP-seq data for CA46 cells. Images of IHC was acquired with a Zeiss Axiomager Z1(Carl Zeiss AG).

Data analysis

Proteome Discovery version 1.3 using the MASCOT search engine was used to analyze mitochondrial protein acetylation data. Sciex PeakView 2.2, MasterView 1.1 and MultiQuant 3.0.2. (AB SCIEX) were used to analyze metabolites of LC-MS data; TopHat2 v2.1.0, Proteome Discover version 1.3 DAVID and Cuffdiff v2.2.1 were used to analyze RNA-seq data; Bowtie2 software (version 2.2.6) and the Integrative Genomics Viewer (IGV) were used to analyze ChIP-seq data. HistoQuest analysis software was used to analyze Images quantification of IHC.

For manuscripts utilizing custom algorithms or software that are central to the research but not yet described in published literature, software must be made available to editors/reviewers. We strongly encourage code deposition in a community repository (e.g. GitHub). See the Nature Research [guidelines for submitting code & software](#) for further information.

Data

Policy information about [availability of data](#)

All manuscripts must include a [data availability statement](#). This statement should provide the following information, where applicable:

- Accession codes, unique identifiers, or web links for publicly available datasets
- A list of figures that have associated raw data
- A description of any restrictions on data availability

Original data of ChIP-seq and RNA-seq in P493 cells are available in the NCBI GEO (accession number GSE124255). Original data of ChIP-seq and RNA-seq in CA46

Field-specific reporting

Please select the one below that is the best fit for your research. If you are not sure, read the appropriate sections before making your selection.

Life sciences Behavioural & social sciences Ecological, evolutionary & environmental sciences

For a reference copy of the document with all sections, see [nature.com/documents/nr-reporting-summary-flat.pdf](https://www.nature.com/documents/nr-reporting-summary-flat.pdf)

Life sciences study design

All studies must disclose on these points even when the disclosure is negative.

Sample size	We determined the sample sizes based on preliminary studies in our laboratories or in similarly published research. The samples were enough to be detected and we saw statistical significant difference in replicated independent experiments. For animal experiments, we used 5 male nude mice for each group and followed the 3 R's of animal research.
Data exclusions	No data were excluded from the data set.
Replication	We defined each sample in different groups performing three independent biological experiments, and the results showed the same trend. For animal studies, we used 5 male nude mice for different groups, and the statistical significance was shown in figures. We confirmed successful replication for our reported data.
Randomization	Mice were randomly allocated to control group or treatment groups..
Blinding	In most experiments, as detailed in the Methods section, samples were analyzed in a blinded manner. Before performing Immunohistochemistry (IHC), the researchers did not know the nature of the samples.

Behavioural & social sciences study design

All studies must disclose on these points even when the disclosure is negative.

Study description	Briefly describe the study type including whether data are quantitative, qualitative, or mixed-methods (e.g. qualitative cross-sectional, quantitative experimental, mixed-methods case study).
Research sample	State the research sample (e.g. Harvard university undergraduates, villagers in rural India) and provide relevant demographic information (e.g. age, sex) and indicate whether the sample is representative. Provide a rationale for the study sample chosen. For studies involving existing datasets, please describe the dataset and source.
Sampling strategy	Describe the sampling procedure (e.g. random, snowball, stratified, convenience). Describe the statistical methods that were used to predetermine sample size OR if no sample-size calculation was performed, describe how sample sizes were chosen and provide a rationale for why these sample sizes are sufficient. For qualitative data, please indicate whether data saturation was considered, and what criteria were used to decide that no further sampling was needed.
Data collection	Provide details about the data collection procedure, including the instruments or devices used to record the data (e.g. pen and paper, computer, eye tracker, video or audio equipment) whether anyone was present besides the participant(s) and the researcher, and whether the researcher was blind to experimental condition and/or the study hypothesis during data collection.
Timing	Indicate the start and stop dates of data collection. If there is a gap between collection periods, state the dates for each sample cohort.
Data exclusions	If no data were excluded from the analyses, state so OR if data were excluded, provide the exact number of exclusions and the rationale behind them, indicating whether exclusion criteria were pre-established.
Non-participation	State how many participants dropped out/declined participation and the reason(s) given OR provide response rate OR state that no participants dropped out/declined participation.
Randomization	If participants were not allocated into experimental groups, state so OR describe how participants were allocated to groups, and if allocation was not random, describe how covariates were controlled.

Ecological, evolutionary & environmental sciences study design

All studies must disclose on these points even when the disclosure is negative.

Study description	Briefly describe the study. For quantitative data include treatment factors and interactions, design structure (e.g. factorial, nested, hierarchical), nature and number of experimental units and replicates.
-------------------	--

Research sample *Describe the research sample (e.g. a group of tagged *Passer domesticus*, all *Stenocereus thurberi* within Organ Pipe Cactus National Monument), and provide a rationale for the sample choice. When relevant, describe the organism taxa, source, sex, age range and any manipulations. State what population the sample is meant to represent when applicable. For studies involving existing datasets, describe the data and its source.*

Sampling strategy *Note the sampling procedure. Describe the statistical methods that were used to predetermine sample size OR if no sample-size calculation was performed, describe how sample sizes were chosen and provide a rationale for why these sample sizes are sufficient.*

Data collection *Describe the data collection procedure, including who recorded the data and how.*

Timing and spatial scale *Indicate the start and stop dates of data collection, noting the frequency and periodicity of sampling and providing a rationale for these choices. If there is a gap between collection periods, state the dates for each sample cohort. Specify the spatial scale from which the data are taken*

Data exclusions *If no data were excluded from the analyses, state so OR if data were excluded, describe the exclusions and the rationale behind them, indicating whether exclusion criteria were pre-established.*

Reproducibility *Describe the measures taken to verify the reproducibility of experimental findings. For each experiment, note whether any attempts to repeat the experiment failed OR state that all attempts to repeat the experiment were successful.*

Randomization *Describe how samples/organisms/participants were allocated into groups. If allocation was not random, describe how covariates were controlled. If this is not relevant to your study, explain why.*

Blinding *Describe the extent of blinding used during data acquisition and analysis. If blinding was not possible, describe why OR explain why blinding was not relevant to your study.*

Did the study involve field work? Yes No

Field work, collection and transport

Field conditions *Describe the study conditions for field work, providing relevant parameters (e.g. temperature, rainfall).*

Location *State the location of the sampling or experiment, providing relevant parameters (e.g. latitude and longitude, elevation, water depth).*

Access and import/export *Describe the efforts you have made to access habitats and to collect and import/export your samples in a responsible manner and in compliance with local, national and international laws, noting any permits that were obtained (give the name of the issuing authority, the date of issue, and any identifying information).*

Disturbance *Describe any disturbance caused by the study and how it was minimized.*

Reporting for specific materials, systems and methods

We require information from authors about some types of materials, experimental systems and methods used in many studies. Here, indicate whether each material, system or method listed is relevant to your study. If you are not sure if a list item applies to your research, read the appropriate section before selecting a response.

Materials & experimental systems

n/a	Involvement in the study
<input type="checkbox"/>	<input checked="" type="checkbox"/> Antibodies
<input type="checkbox"/>	<input checked="" type="checkbox"/> Eukaryotic cell lines
<input checked="" type="checkbox"/>	<input type="checkbox"/> Palaeontology
<input type="checkbox"/>	<input checked="" type="checkbox"/> Animals and other organisms
<input type="checkbox"/>	<input checked="" type="checkbox"/> Human research participants
<input checked="" type="checkbox"/>	<input type="checkbox"/> Clinical data

Methods

n/a	Involvement in the study
<input type="checkbox"/>	<input checked="" type="checkbox"/> ChIP-seq
<input checked="" type="checkbox"/>	<input type="checkbox"/> Flow cytometry
<input checked="" type="checkbox"/>	<input type="checkbox"/> MRI-based neuroimaging

Antibodies

Antibodies used

The following primary antibodies were used (primary antibody; clone name; cat number; lot number; company; dilution):
 Myc Monoclonal (Clone 9E10); cat:sc40; lot: A1519; santa curz (1:3000)
 Myc Monoclonal (Clone 9E10); cat: MA1-980 lot: 33206 Zymed, Invitrogen (1:3000)
 Myc Monoclonal (Clone EP121); cat:ZA0555; lot:17610309; ZSGB-BIO (Do not dilute)
 BCAT1 Monoclonal (Clone 3F5); cat:ab195663; lot:GR239295-5; Abcam (1:1000)
 SCD Monoclonal (Clone CD.E10); cat:NB600-1133; lot:14685; Novus Biologicals (1:1000)
 β -Tubulin Monoclonal (Clone C66); cat:M20005; lot:254283; Abmart (1:3000)
 KDM5A Monoclonal(Clone D28B10); cat:3876; lot:1; Cell Signaling Technology (1:1000)
 H3K4me3 Monoclonal(Clone C42D8); cat:9751; lot:10; Cell Signaling Technology (1:2000)

H3K4me2 Monoclonal (Clone C54G9); cat:9725; lot:9; Cell Signaling Technology (1:1000)
 H3K4me1 Monoclonal (Clone D1A9); cat:5326; lot:3; Cell Signaling Technology (1:1000)
 H3K79me2 Monoclonal (Clone D15E8); cat:5427; lot:3; Cell Signaling Technology (1:1000)
 H3K9me2 Monoclonal (Clone D85B4); cat: 4658; lot:2; Cell Signaling Technology (1:1000)
 H3K27me3 Monoclonal (Clone C36B11); cat:9733; lot:8; Cell Signaling Technology (1:1000)
 SIRT3 Monoclonal (Clone C73E3) cat:2627; lot:8; Cell Signaling Technology (1:1000)
 Flag-M2 Monoclonal (Clone M2); cat:F1804; lot:SLBK1346V; Sigma-Aldrich (1:3000)
 HA Monoclonal (Clone HA-7); cat:H9658; lot:024M4773; Sigma-Aldrich (1:2000)
 Pan-acetyl-lysine Polyclonal; cat:9441; lot:12; Cell Signaling Technology (1:500)
 SDHA Polyclonal; cat:14865-1-AP; lot:00050301; Proteintech (1:1000)
 SKP2 Polyclonal; cat:15010-1-AP; lot:0006215; Proteintech (1:1000)
 ACAT1 Polyclonal; cat:16215-1-AP; lot:0007657; Proteintech (1:1000)
 SLC7A5 Polyclonal; cat:5347; lot:3; Cell Signaling Technology (1:1000)
 ENO1 Polyclonal; cat: 11204-1-AP; lot:00014144; Proteintech (1:1000)
 LDHA Polyclonal; cat:19987-1-AP; lot:00015375; Proteintech (1:1000)
 NPM1 Polyclonal cat:60096-1-Ig; lot:10000620; Proteintech (1:1000)
 Ubiquitin Polyclonal cat:10201-2-AP; lot:0023129; Proteintech (1:500)
 Calreticulin Polyclonal cat:10292-1-AP; lot:0018874; Proteintech (1:1000)
 COX4 Polyclonal cat:11242-1-AP; lot:00081701; Proteintech (1:1000)
 LaminB1 Polyclonal cat:12987-1-AP; lot:0003803; Proteintech (1:1000)
 KDM5B Polyclonal cat:A7772; lot:0204110201; Abclonal(1:1000)
 KDM5C Polyclonal cat: 14426-1-AP; lot: 00015804; Proteintech (1:1000)
 KDM5D Polyclonal cat: 22739-1-AP; lot: 00019498; Proteintech (1:1000)
 H3K4me3 Polyclonal cat: 07-473; lot:2839113; Millipore (1:2000)
 H3 Polyclonal; cat: ab1791; lot:GR30598-2; Abcam (1:2000)
 SIRT4 Polyclonal; cat:21440-1-AP; lot:0014381; Proteintech (1:1000)
 SIRT5 Polyclonal; cat:15122-1-AP; lot:0006365; Proteintech (1:1000)
 SDHA-K335Ac Polyclonal; the antibody was generated by immunization of rabbits at Abclonal Co., Ltd. (1:1000)
 V5 Polyclonal; cat:ab9116; lot:130627; Abcam (1:1000)
 spike-in antibody Polyclonal; cat:61686; lot:00419007; Active Motif (1:2000)

Validation

These antibodies have either been validated in published literatures, which are cited in the Methods. Moreover, we also validated the antibodies by Western blot using specific targeting shRNAs or over-expressing vectors. The manufacturer's website, relevant citations and antibody profiles were provided in Method in supplementary Tables 6.

Eukaryotic cell lines

Policy information about [cell lines](#)

Cell line source(s)

HEK293T and HeLa cells from ATCC;
 HT1080 and Raji cells from Chinese Academy of Sciences, Shanghai;
 The human P493-6 B cell line (a gift from Chi V. Dang's lab)
 CA46 cells from Cobioer, Nanjing

Authentication

Cell line identities were confirmed by STR fingerprinting.

Mycoplasma contamination

All cell lines were tested routinely to make sure they are negative for mycoplasma contamination by Mycoplasma PCR method.

Commonly misidentified lines
(See [ICLAC](#) register)

No commonly misidentified cell lines were used.

Palaeontology

Specimen provenance

Provide provenance information for specimens and describe permits that were obtained for the work (including the name of the issuing authority, the date of issue, and any identifying information).

Specimen deposition

Indicate where the specimens have been deposited to permit free access by other researchers.

Dating methods

If new dates are provided, describe how they were obtained (e.g. collection, storage, sample pretreatment and measurement), where they were obtained (i.e. lab name), the calibration program and the protocol for quality assurance OR state that no new dates are provided.

Tick this box to confirm that the raw and calibrated dates are available in the paper or in Supplementary Information.

Animals and other organisms

Policy information about [studies involving animals](#); [ARRIVE guidelines](#) recommended for reporting animal research

Laboratory animals

5-week-old male BALB/c nude mice (n = 5 for each group) (SJA Laboratory Animal Company, China).

Wild animals

not used

Field-collected samples

no field-collected samples

Ethics oversight

All animal studies were conducted with approval from the Animal Research Ethics Committee of University of Science and Technology of China.

Note that full information on the approval of the study protocol must also be provided in the manuscript.

Human research participants

Policy information about [studies involving human research participants](#)

Population characteristics

The primary DLBCLs and control lymph node specimens obtained from 85 patients were randomly selected from the archives of the First Affiliated Hospital of Anhui Medical University. Among them, 55 patients were diagnosed with DLBCL, and the other 30 patients were diagnosed with other diseases than lymphoma. Of the 55 patients (DLBCLs), 25 were women and 30 were men, with 36 patients over the age of 50. Of the 30 patients (no lymphoma), 16 were women and 14 were men, with 15 patients over the age of 50. (If necessary, we will provide the information as a supplementary table in the manuscript.)

Recruitment

We selected the samples of patients diagnosed with large B lymphoma for immunohistochemical experiments, which were mainly from 2015 to 2017. At the same time, normal tissue samples were obtained from patients who were not diagnosed as lymphoma from 2015 to 2017. For use of these clinical materials for research purposes, prior patients' written informed consents and approval from the Institutional Research Ethics Committee of the First Affiliated Hospital of Anhui Medical University were obtained.

Ethics oversight

Ethical approval for the studies was obtained from the Institutional Research Ethics Committee of the First Affiliated Hospital of Anhui Medical University

Note that full information on the approval of the study protocol must also be provided in the manuscript.

Clinical data

Policy information about [clinical studies](#)

All manuscripts should comply with the ICMJE [guidelines for publication of clinical research](#) and a completed [CONSORT checklist](#) must be included with all submissions.

Clinical trial registration

Provide the trial registration number from [ClinicalTrials.gov](#) or an equivalent agency.

Study protocol

Note where the full trial protocol can be accessed OR if not available, explain why.

Data collection

Describe the settings and locales of data collection, noting the time periods of recruitment and data collection.

Outcomes

Describe how you pre-defined primary and secondary outcome measures and how you assessed these measures.

ChIP-seq

Data deposition

Confirm that both raw and final processed data have been deposited in a public database such as [GEO](#).

Confirm that you have deposited or provided access to graph files (e.g. BED files) for the called peaks.

Data access links

May remain private before publication.

Original data of ChIP-seq in P493 cells are available in the NCBI GEO (accession number GSE124255).
Data access links: <https://www.ncbi.nlm.nih.gov/geo/query/acc.cgi?acc=GSE124255>
Original data of ChIP-seq in CA46 cells are available in the NCBI GEO (accession number GSE141227).
Data access links: <https://www.ncbi.nlm.nih.gov/geo/query/acc.cgi?acc=GSE141227>

Files in database submission

P493 cells:
processed data file: DMS_1-peaks.bed (ChIP-seq-tet-DMS)
DMS_2-peaks.bed (ChIP-seq -tet+DMS)
DMS_3-peaks.bed (ChIP-seq +tet-DMS)
DMS_4-peaks.bed (ChIP-seq +tet+DMS)
Input_bed.bed (Input-tet-DMS)
raw data file: DMS_1.fq.gz (ChIP-seq-tet-DMS)
DMS_2.fq.gz (ChIP-seq -tet+DMS)
DMS_3.fq.gz (ChIP-seq +tet-DMS)
DMS_4.fq.gz (ChIP-seq +tet+DMS)
Input.fq.gz (Input-tet-DMS)
CA46 cells:
processed data file: spike-in_IP_1_peaks.bw (spike-in_ChIP-seq_NTC-DMS)
spike-in_IP_2_peaks.bw (spike-in_ChIP-seq_NTC+DMS)
spike-in_IP_3_peaks.bw (spike-in_ChIP-seq_shMyc-DMS)
spike-in_IP_4_peaks.bw (spike-in_ChIP-seq_shMyc+DMS)
spike-in_Input_peaks.bw (spike-in_Input_NTC-DMS)
raw data file: spike-in_IP_1_1_clean.fq.gz (spike-in_ChIP-seq_NTC-DMS)

spike-in_IP_1_2. clean.fq.gz (spike-in_ChIP-seq_NTC-DMS)
 spike-in_IP_2_1. clean..fq.gz (spike-in_ChIP-seq_NTC+DMS)
 spike-in_IP_2_2. clean..fq.gz (spike-in_ChIP-seq_NTC+DMS)
 spike-in_IP_3_1. clean.fq.gz (spike-in_ChIP-seq_shMyc-DMS)
 spike-in_IP_3_2. clean.fq.gz (spike-in_ChIP-seq_shMyc-DMS)
 spike-in_IP_4_1. clean.fq.gz (spike-in_ChIP-seq_shMyc+DMS)
 spike-in_IP_4_2. clean.fq.gz (spike-in_ChIP-seq_shMyc+DMS)
 spike-in_Input_1_1. clean.fq.gz (spike-in_Input_NTC-DMS)
 spike-in_Input_1_2. clean.fq.gz (spike-in_Input_NTC-DMS)

Genome browser session
 (e.g. [UCSC](#))

We just updated our ChIP-seq data to the GEO, and have not submitted to the Genome browser session.

Methodology

Replicates

For ChIP-seq assay, one replicate was used for P493 or CA46 cells each.

Sequencing depth

Sequencing depth of ChIP-seq in P493 cell: Input group: clean reads: 12,283,316; -tet -DMS group: clean reads: 10,572,686; -tet +DMS group: clean reads: 11,318,239; +tet -DMS group: clean reads: 11,371,480; +tet +DMS group: clean reads: 10,779,763
 Sequencing depth of ChIP-seq in CA46 cell: Input group: clean reads: 19,077,338; -tet -DMS group: clean reads: 23,993,059; -tet +DMS group: clean reads: 31,183,123; +tet -DMS group: clean reads: 26,144,884; +tet +DMS group: clean reads: 30,358,612

Antibodies

H3K4me3 antibody (Millipore, 07-473) were used in P493 cells for ChIP-seq.
 H3K4me3 antibody (Millipore, 07-473) and spike-in antibody (Active Motif, 61686) were used in CA46 cells for ChIP-seq.

Peak calling parameters

Sequenced reads were mapped to the UCSC human genome hg19 using software Bowtie 2 (version 2.2.6). Aligned reads were used for subsequent generation of binding profiles, peak callings, motif analyses and traveling ratio analyses. MACS (version 1.4.2) was used for peak callings from the aligned reads

Data quality

Clean Reads Q20 Rate of ChIP-seq in P493 cells: Input group: 99.10%; -tet -DMS group: 98.85%; -tet +DMS group: 98.87%; +tet -DMS group: 98.82%; +tet +DMS group: 98.78%
 Clean Reads Q20 Rate of ChIP-seq in CA46 cells:
 Input group: 97.35%; -tet -DMS group: 97.26%; -tet +DMS group: 97.27%; +tet -DMS group: 97.37%; +tet +DMS group: 97.23%

Software

HOMER(version 4.10) ; Bowtie2 software (version 2.2.6); the Integrative Genomics Viewer (IGV).

Flow Cytometry

Plots

Confirm that:

- The axis labels state the marker and fluorochrome used (e.g. CD4-FITC).
- The axis scales are clearly visible. Include numbers along axes only for bottom left plot of group (a 'group' is an analysis of identical markers).
- All plots are contour plots with outliers or pseudocolor plots.
- A numerical value for number of cells or percentage (with statistics) is provided.

Methodology

Sample preparation

Describe the sample preparation, detailing the biological source of the cells and any tissue processing steps used.

Instrument

Identify the instrument used for data collection, specifying make and model number.

Software

Describe the software used to collect and analyze the flow cytometry data. For custom code that has been deposited into a community repository, provide accession details.

Cell population abundance

Describe the abundance of the relevant cell populations within post-sort fractions, providing details on the purity of the samples and how it was determined.

Gating strategy

Describe the gating strategy used for all relevant experiments, specifying the preliminary FSC/SSC gates of the starting cell population, indicating where boundaries between "positive" and "negative" staining cell populations are defined.

- Tick this box to confirm that a figure exemplifying the gating strategy is provided in the Supplementary Information.

Magnetic resonance imaging

Experimental design

- Design type
- Design specifications
- Behavioral performance measures

Acquisition

- Imaging type(s)
- Field strength
- Sequence & imaging parameters
- Area of acquisition
- Diffusion MRI Used Not used

Preprocessing

- Preprocessing software
- Normalization
- Normalization template
- Noise and artifact removal
- Volume censoring

Statistical modeling & inference

- Model type and settings
- Effect(s) tested
- Specify type of analysis: Whole brain ROI-based Both
- Statistic type for inference (See [Eklund et al. 2016](#))
- Correction

Models & analysis

- n/a Involved in the study
- Functional and/or effective connectivity
- Graph analysis
- Multivariate modeling or predictive analysis
- Functional and/or effective connectivity
- Graph analysis

